NASA

Technical Memorandum 79711

# Contributions to the Fourth Solar Wind Conference

## Burghausen, Federal Republic of Germany

**August 28 - September 1, 1978**

## Laboratory for Extraterrestrial Physics



**FEBRUARY 1979**

National Aeronautics and
Space Administration

**Goddard Space Flight Center**
Greenbelt, Maryland 20771

CONTRIBUTIONS TO THE FOURTH SOLAR WIND CONFERENCE

Burghausen, Federal Republic of Germany

August 28 - September 1, 1978

NASA/Goddard Space Flight Center
Laboratory for Extraterrestrial Physics
Greenbelt, MD 20771

TO BE PUBLISHED IN: Solar Wind IV

TABLE OF CONTENTS

# INITIAL RESULTS FROM THE VOYAGERS 1, 2 MAGNETIC FIELD EXPERIMENTS

M. H. Acuna, L. F. Burlaga,
R. P. Lepping and N. F. Ness
Laboratory for Extraterrestrial Physics
Goddard Space Flight Center
Greenbelt, Maryland 20771

## 1. Introduction

The aim of this paper is to survey some of the initial results obtained with the Goddard Space Flight Center magnetic field experiments aboard Voyagers 1 and 2. We consider the period from launch in August 1977 to March 1978, when the spacecraft moved from 1 AU to 2.5 AU. A plot of the trajectories is given in the paper of Belcher et al., which appears in these proceedings.

The interplanetary magnetic field observations on each spacecraft are made with a dual magnetometer system, described by Behannon et al. (1978). The Principal Investigator is N. F. Ness. Vector magnetic field measurements are made at a rate of 16.66 samples/s (every 60 milliseconds), allowing a detailed study of small scale phenomena such as shocks. At high bit rates, all of the measurements are transmitted, while at the lowest data rates 1.92 second averages of the field are transmitted. Since the spacecraft are always in the solar wind, mesoscale and macroscale phenomena can also be investigated, the only interruptions being due to limits on the telemetry coverage. The complex task of data reduction is carried out jointly for the plasma science and the magnetic field experiments at GSFC, so plasma and magnetic field data are simultaneously available for analysis in a common format. Dr. H. Bridge, the Principal Investigator of the plasma experiment, and two of his Co-Investigators at MIT, J. Belcher and J. Sullivan, provided the plasma data that appear below.

The plan of this paper is to: discuss some large-scale characteristics of the interplanetary magnetic field in the period August 1977-March 1978; describe a characteristic of a post-shock flow; and analyze the detailed structures of three types of interplanetary shocks.

## 2. Large-Scale Structure

Hourly averages of the magnetic field intensity (B) and direction ($\lambda, \delta$) are shown in Figures 1 and 2 for two consecutive solar rotations. The angles $\lambda$ and $\delta$ are measured in heliographic (RTN) spacecraft centered coordinates: $\delta$ is the latitude measured with

respect to the RT plane, ($\hat{R}$ points away from the sun; $\hat{T}$ lies in a plane parallel to the solar equator and points in the direction of the sun's rotation); $\lambda$ is the longitude, which is zero when the field points along $\hat{R}$ and which increases counterclockwise when viewed from the north.

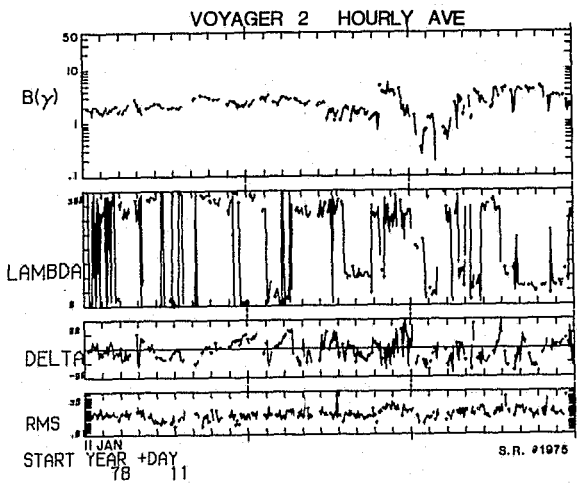


FIGURE 1

The magnetic field variations in Figures 1 and 2 are very different from the stable, recurrent two sector pattern observed by Pioneers 10 and 11 when they moved through the same heliocentric radial distance range in 1972/1973 (Smith and Wolfe, 1977). Most significantly, large, recurrent sectors do not appear in the Voyager data. Small regions of uniform polarity can be seen in Figure 1, but they do not recur on the following solar rotation (Figure 2) with the same general characteristics. There are several intervals in which the magnetic field does not lie near the nominal spiral direction ($\lambda_{ss}$ 135° or 315° at 1 AU for negative or positive polarization). The magnetic field intensity profile in Figures 1 and

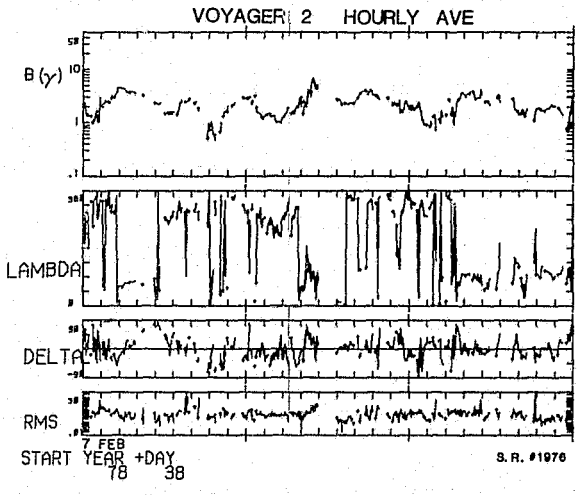


FIGURE 2

2 is likewise irregular and non-recurrent. (Note the logarithmic scale.) For example, exceptionally low intensities were observed on January 29 (Figure 1), but they did not recur on the following rotation. Similarly, exceptionally low intensities were observed on February 14 (Figure 2), but they were not observed 27 days earlier. In general, the magnetic field intensity varies more on SR 1976 than on SR 1975.

The results in Figures 1 and 2 are representative of the large-scale fields observed by Voyagers 1 and 2, i.e., the magnetic field intensity and direction are irregular and they usually do not show simple, recurrent patterns. The reason that the Voyager results are so different from the Pioneer results is probably associated with the phase of the solar cycle. The Voyager observations were made during an increase of solar activity, when there were many active regions at mid-latitudes and few large, stable coronal holes near the equator. The corresponding Pioneer observations were made in the declining phase of the solar cycle, when activity was low and large, and stable coronal holes were present near the equator.

3. A Post-Shock Flow

A shock and post-shock flow were observed near 1 AU by Voyagers 1 and 2 and by Earth orbiting IMPs 7 and 8 in the period September 19 to 21, 1977, when the Voyager 1-sun-earth angle was $4.2^{\circ}$ and the Voyager 2-sun-Voyager 1 angle was $4.3^{\circ}$ as shown in Figure 3. The multiple spacecraft configuration was ideal for studying azimuthal gradients, i.e., in the direction normal to the earth-sun line. Behind the shock at Voyager 2 (0507 U.T., September 20), indicated by the abrupt increase in speed V and magnetic field intensity B in Figure 3, the speed and field intensity decreased monotonically to the preshock

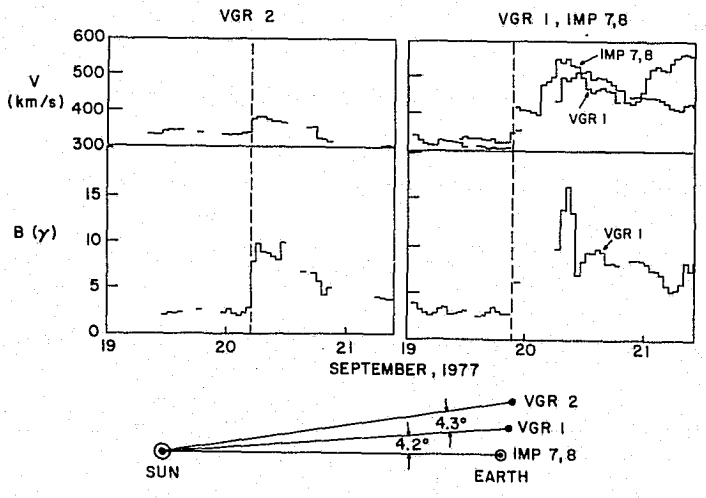


FIGURE 3

values $\lesssim$ 20 hrs later. In contrast, behind the shock observed at Voyager 1 (2130 U.T. $\pm$ 50 m, September 19) the speed and field increased for several hours before decreasing to the preshock values. In other words, the post-shock speed and magnetic field intensity profiles at Voyager 2 resembled a blast wave or F-type shock (Hundhausen, 1972), while the profiles behind the shock at Voyager 1, just $4.2^{o}$ away, resembled a driven wave or R-type shock (Hundhausen, 1972). The speed profile at IMPs 7 and 8 was similar to that at Voyager 1.

Our interpretation of these observations is that the shock was driven by a piston with a thin lateral boundary. The piston passed Voyager 1 and IMP, but it did not extend far enough in the azimuthal direction to intercept Voyager 2. Thus, the width of the boundary was less than $4.3^{o}$.

4. Shock Structure

Voyagers 1 and 2 observed more than 20 shocks in the 6 months interval under consideration. Here, only three shocks will be discussed: a perpendicular forward shock ($\underset{\sim}{B}$ perpendicular to the shock normal, and the shock moving away from the sun relative to the unshocked plasma); an oblique forward shock; and a quasi-parallel reverse shock (moving toward the sun relative to the unshocked plasma). Table 1 gives the basic parameters just before and after each shock.

Perpendicular forward shock. Figure 4 shows the shock mentioned above, observed at Voyager 2 at 0507 UT on September 20, 1977 at 1.05 AU. The data are 1.92s averages obtained in the low bit rate mode. Two characteristics of the data in this figure identify the event as a quasi-perpendicular shock: 1) the large,

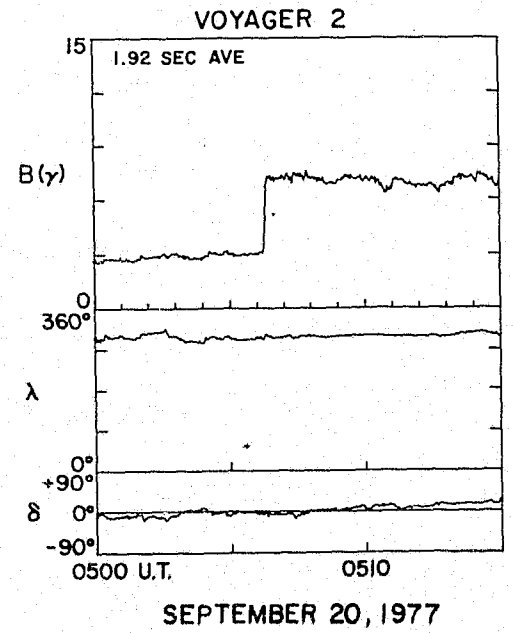


FIGURE 4

abrupt increase in the magnetic field intensity such that $B_2/B_1 = n_2/n_1$ (see Table 1 and Burlaga, 1971), and 2) the absence of any significant change in the direction of $\underline{B}$. Given $V_1$, $V_2$, and $B_2/B_1 = n_2/n_1$ one can use the mass conservation equation to obtain the shock speed, viz., U = 400 km/s, or $U-V_1$ = 60 km/s relative to the solar wind ahead of the shock.

A full least squares fit to a subset of the Rankine-Hugoniot conservation relations (Lepping and Argentiero, 1971) yielded the normal orientation as $\lambda_n = 29.1^o$, $\delta_n = -11.2^o$ with a rest frame shock speed of 382 km/sec. The corresponding angle between the best fit pre-shock field and the normal was $88^o$ thus confirming the perpendicular character of this shock. The "quality factor" normally associated with this calculation was 0.74 (where unity corresponds to an excellent fit) indicating a good fit. Using a time delay calculation between the sudden commencement time (1142 U.T. on 19 September) at earth and the shock passage at Voyager 2 reasonably consistent results were obtained: $V_S$ = 310 km/s, $\lambda_n = 27^o$, $\delta_n = -2^o$. The slightly lower shock speed (19%) may be explained by local shock curvature in the Earth-Voyager region, consistent with the limited extent of the associated driver plasma.

The structure of the shock is simple. There are no fluctuations upstream; the intensity increased in a very short time in the main shock transition, and behind the shock there are random fluctuations of very small amplitude.

Oblique forward shock. An oblique forward fast shock was observed at Voyager 2 at 1655:10 UT on February 2, 1978. High resolution magnetic field data (60 ms samples) in Figure 5 show an abrupt increase in B, which is characteristic of a shock. Simultaneous increases in the plasma parameters were also observed

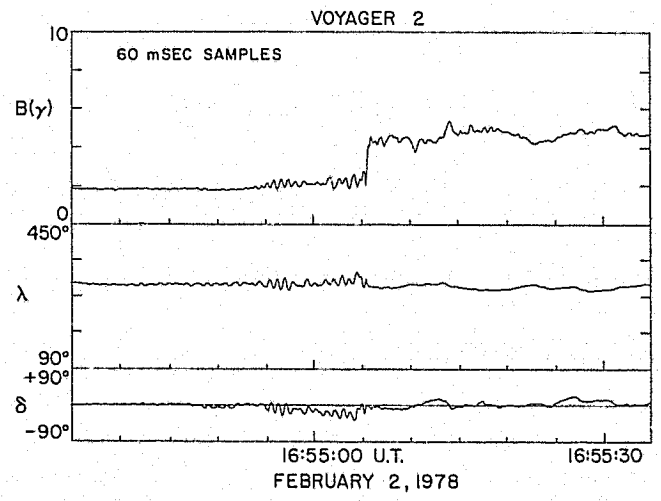


FIGURE 5

(see Table 1), confirming that the event was probably a forward shock. The direction of the magnetic field changed slightly across the shock, indicating that the shock was oblique. One can use the coplanarity theorem to calculate the shock normal (e.g., see Hundhausen, 1972). The angle between the shock normal and the upstream magnetic field was $47^{\circ}$. The speed of the shock with respect to the upstream solar wind was $U-V_1 = 102$ km/s.

The structure of the oblique shock shown in Figure 5 is somewhat more complicated than that of the perpendicular shock described above, but it is not turbulent. Wave packets with quasi-sinusoidal, high frequency fluctuations appear upstream of the shock transition, and lower frequency fluctuations appear downstream.

Figure 6 shows power spectra in the range (0-8) Hz for the undisturbed upstream region (A), the region just ahead of the shock (B), and a region behind the shock (C). Spectrum C shows appreciable low frequency power with respect to the background (Spectrum A), but no spectral peak is evident. Spectrum B shows a distinct peak at ≈ 1.2 Hz in the 5-second interval ahead of the shock, corresponding to the quasi-periodic fluctuations evident in Figure 5.

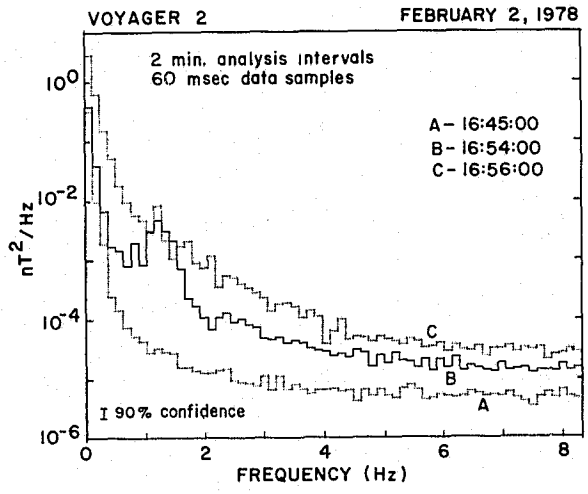




FIGURE 6

A polarization analysis for the quasi-periodic fluctuations just ahead of the shock showed that the fluctuations are nearly circular RH polarized waves propagating $40^{\circ}$ with respect to the ambient magnetic field. This is shown in the holograph of Figure 7 which gives a plot of the perturbation vector in the maximum variance plane; the wave vector, $\underset{\sim}{k}$, and the component of $\underset{\sim}{B}$ parallel to $\underset{\sim}{k}$ are normal to the plane of this figure and point into the paper. Waves such as these have been observed upstream of the earth's bow shock. Greenstadt et al. (1975) and Fairfield and Feldman (1975) identified

them as whistler waves. Taking advantage of the successive inward and outward motion of the bow shock, they showed that the bow shock whistlers were standing waves. Their technique cannot be applied to an interplanetary shock, which locally moves in just one direction. On the other hand, the fast, uniform, known motion of interplanetary shocks offers the advantage that scale lengths can be determined more precisely.

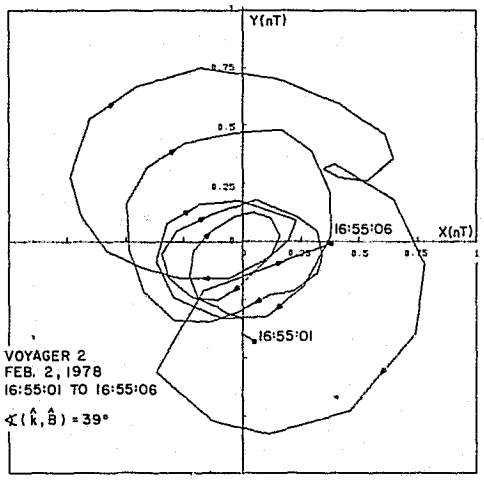


FIGURE 7

Quasi-parallel, reverse shock. Figure 8 shows an unusual event, recorded by Voyager 2 at 0920 UT on January 29, 1978. There is a large abrupt decrease in density and proton thermal speed (temperature) and a slight decrease in magnetic field intensity coincident with an abrupt increase in bulk speed. This is the signature of a reverse, fast shock (e.g., see Burlaga, 1971).

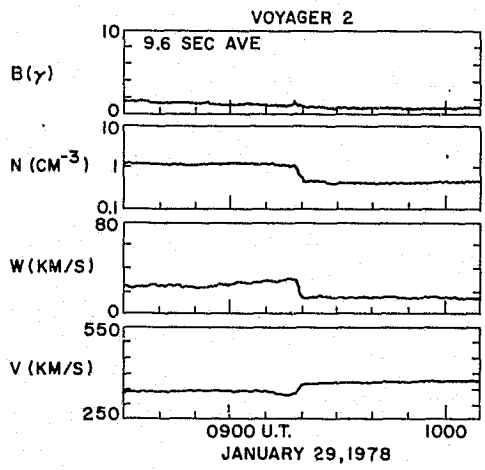


FIGURE 8

High resolution (1.92s) magnetic field data in Figure 9 show a small change in magnetic field direction ($\lambda$) and a small increase in

intensity (B) at 0919 UT, which is the main transition in the shock. The small size of $\Delta\lambda$ and $\Delta B$ indicates that the shock is quasi-parallel (for a parallel shock $\Delta\lambda = \Delta B = 0$).

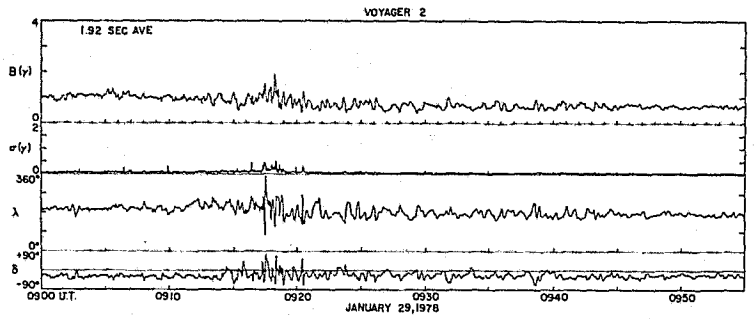


FIGURE 9

The structure of this shock differs appreciably from that of the perpendicular and oblique shocks discussed above. Upstream (late times), there are low frequency, irregular fluctuations extending > 500,000 km from the shock. A preliminary power spectral and polarization analysis reveals these fluctuations to be left hand, elliptically polarized waves with characteristic periods of 20-25 seconds. The main shock transition is turbulent, with large amplitude fluctuations in both intensity and direction; these fluctuations extend to high frequencies, as indicated by the high variance of the 60 ms measurements of the magnetic field components in Figure 9. Downstream (early times--in the shocked plasma) there are high frequency, turbulent fluctuations extending > 250,000 km behind the shock. Power spectral and polarization analyses indicate that these fluctuations are right-hand, nearly circular-polarized waves with characteristic periods of 6 to 12 seconds, the period decreasing as we approach the main shock transition.



## 5. Summary

Some early results of the Voyager 1 and 2 magnetic field measurements between 1 AU and 2.5 AU were surveyed.

In the macroscale data (> 27 days) it was noted that the magnetic field intensities and sector patterns were complex and variable, in contrast to the simple and stable patterns oberved in the same region (1.0 to 2.5 A.U.) by Pioneer 10 and 11 during 1974.

On a smaller scale, the flow configuration behind the September 14-21, 1978 shock was investigated using magnetic field and plasma

data from Voyagers 1 and 2 and from IMP 7 and 8. The shock was driven by a piston and the azimuthal boundary of the piston was found to be very thin at 1 A.U.

The structures of three different types of interplanetary shocks were analyzed. A perpendicular forward shock was found to be thin and laminar, with almost no fluctuations upstream and downstream. An oblique forward shock was found to be thin, with whistler wave packets upstream and higher intensity turbulent fluctuations downstream. A quasi-parallel, reverse shock was found to be turbulent, with irregular, LH, elliptical-polarized fluctuations extending >500,000 km upstream, and with the nearly circular-polarized waves extending > 250,000 km downstream.

TABLE 1
Shock Characteristics

| Event at Voyager 2 | $B_1$ | $B_2$ | $n_1$ | $n_2$ | $T_1$ | $T_2$ | $V_1$ | $V_2$ |
|---|---|---|---|---|---|---|---|---|
| Sept. 20, 1977 | 3.1 | 6.8 | 9.1 | 19.8 | 2.4 | 4.5 | 341 | 381 |
| Feb. 2, 1978 | 2.3 | 4.3 | 1.7 | 4.0 | 1.4 | 3.8 | 335 | 390 |
| Jan. 29, 1978 | 0.7 | 1.2 | 0.5 | 1.2 | 1.0 | 5.4 | 370 | 330 |

(B is in gammas, n in $cm^{-3}$, T in $10^{4o}K$, and V in km/s)

REFERENCES

Behannon, K.W., M.H. Acuna, L.F. Burlaga, R. P. Lepping, N.F. Ness and F. M. Neubauer, Magnetic field experiment for Voyagers 1 and 2, Space Sci. Rev., 21, 235, 1977.

Burlaga, L.F., Hydromagnetic waves and discontinuities in the solar wind, Space Sci. Rev., 12, 600, 1971.

Fairfield, D.H. and W.C. Feldman, Standing waves at low Mach number laminar bow shocks, J. Geophys. Res., 80, 515, 1975.

Greenstadt, E.W., C.T. Russell, F.L. Scarf, V. Formisano, and M. Neugebauer, Structure of the quasi-perpendicular laminar bow shock, J. Geophys. Res., 80, 502, 1975.

Hundhausen, A.J., Coronal Expansion and Solar Wind, Springer, New York, 1972.

Lepping, R.P. and P. D. Argentiero, Single spacecraft method of estimating shock normals, J. Geophys. Res., 76, 4349, 1971.

Smith, E.J. and J. H. Wolfe, Pioneer 10, 11 observations of evolving solar wind streams and shocks beyond 1 AU, p. 227, in Study of Travelling Interplanetary Phenomena, 1977, eds., M.A. Shea et al., D. Reidel Publishing Co., Dordrecht-Holland, 1977.

# ALFVÉN WAVES AND ALFVÉNIC FLUCTUATIONS IN THE SOLAR WIND

K.W. Behannon and L.F. Burlaga
Laboratory for Extraterrestrial Physics
Goddard Space Flight Center
Greenbelt, Maryland 20771, USA

Abstract Recent measurements have confirmed that fluctuations in the bulk velocity of the solar wind are correlated with fluctuations in the magnetic field more than one-third of the time and that these observed "Alfvénic" fluctuations have several characteristics in common with Alfvén waves. They are not "pure" Alfvén waves because there are fluctuations in magnetic intensity, and at times tangential discontinuities are also present. Because the fluctuations in $\underset{\sim}{B}$ are three-dimensional, they are most consistent with being general Alfvén waves, although they are usually found to be "nearly" transverse. The assumption that the observed waves are plane waves may not be valid over distances $\gtrsim$ 0.01 AU. A better theoretical understanding is needed with respect to mode-coupling, stability, and propagation.

## 1. INTRODUCTION

Although the interplanetary magnetic field has a spiral configuration on average, there are always fluctuations in it on scales of an hour or more. In general, these fluctuations are complex and are the result of many different physical processes. There is a relatively simple subset of these fluctuations which occurs more than one third of the time and is characterized by a high correlation between fluctuations in the bulk velocity $\underset{\sim}{v}$ and the magnetic field $\underset{\sim}{B}$. These are called Alfvénic fluctuations. Alfvénic fluctuations are important for several reasons: they scatter cosmic rays; they modify heat transport; they influence geomagnetic activity; they may carry information on the fundamental acceleration process of the solar wind; and their relative simplicity offers the hope that their physical nature can be understood, thus contributing to a better understanding of a fundamental plasma.

The subject of Alfvén waves has been discussed in several reviews during the past few years (Hollweg, 1974, 1975, 1978; Barnes, 1974; Völk, 1975) which were written from a theoretical point of view. A comprehensive, balanced review of the theory and observations of Alfvén waves and Alfvénic fluctuations was recently written by Barnes (1978). In this present review we attempt to give a concise account of the basic types of Alfvén waves that are possible and a summary of the observations of Alfvénic fluctuations that have been made using both magnetic field and plasma data. We shall tend to stress the ways in which Alfvénic

fluctuations (AF's) differ from pure transverse Alfvén waves (TAW's), in the hope that it will stimulate fresh thinking and new progress in solar wind and wave studies. We shall also show the ways in which AF's resemble TAW's.

## 2. BASIC TYPES OF ALFVEN WAVES

"Alfvén wave" is a general term covering several different possible types of magnetic field and plasma fluctuations. Necessary conditions for an Alfvén wave of any type include the following.

1. $\underset{\sim}{B}(t)$ can be written as the sum of an unperturbed component $\underset{\sim}{B}_o$ and the wave perturbation $\underset{\sim}{B}_1$:

$$\underset{\sim}{B} = \underset{\sim}{B}_o + \underset{\sim}{B}_1. \tag{1}$$

   Note that $\langle \underset{\sim}{B} \rangle = \underset{\sim}{B}_o$ if and only if $\langle \underset{\sim}{B}_1 \rangle = 0$, and $\langle \underset{\sim}{B}_1 \rangle$ is not necessarily zero in general (here $\langle\ \rangle$ denotes the average).

2. The wave moves along $\underset{\sim}{B}_o$ at the speed

$$V_{A_o} = B_o/\sqrt{4\pi\rho}, \tag{2}$$

   where $\rho$ is the density.

3. There is a perturbation in bulk velocity, $\underset{\sim}{V}_1$, which is related to $\underset{\sim}{B}_1$ by the equation

$$\underset{\sim}{V}_1 = \pm\, (V_{A_o}/B_o)\, \underset{\sim}{B}_1. \tag{3}$$

   The minus sign refers to waves moving in the $\hat{B}_o = \underset{\sim}{B}_o/B_o$ direction.

4. The waves satisfy a linear wave equation. Both large amplitude Alfvén waves ($B_1 \sim B_o$) and small amplitude Alfvén waves ($B_1 << B_o$) are linear waves in this sense. The instantaneous Poynting flux for an Alfvén wave is

$$\underset{\sim}{S} = \frac{c}{4\pi}\ \underset{\sim}{E}\times\underset{\sim}{B} = -\frac{1}{4\pi}\ (\underset{\sim}{V}_1\times\underset{\sim}{B}_o)\times(\underset{\sim}{B}_o\times\underset{\sim}{B}_1), \tag{4}$$

   where $\underset{\sim}{V}_1$ is given by (3). $\underset{\sim}{S}$ can be written as

$$\underset{\sim}{S} = -\frac{V_{A_o}}{4\pi}\left[(B_{1\perp})^2\,\hat{B}_o - B_{1\parallel}\ \underset{\sim}{B}_{1\perp} + B_o\,\underset{\sim}{B}_{1\perp}\right]. \tag{5}$$

The last term may be written as $\left[B_0^2/(4\pi)\right] \underset{\sim}{V}_{1\perp}$, which represents a convection of the unperturbed field energy by the perturbation velocity normal to $\underset{\sim}{B}_0$. For waves which are periodic, the last two terms in (5) average to zero, and the average Poynting flux in a wave packet is

$$\langle \underset{\sim}{S} \rangle = - \frac{V_{A_0}}{4\pi} (B_{1\perp})^2 \hat{B}_0. \tag{6}$$

Since $V_{A_0} = V_A \cos\theta$, where $V_A = B/\sqrt{4\pi\rho}$ and $\theta$ is the angle between $\underset{\sim}{B}_0$ and $\underset{\sim}{B}$, one can write (6) in the form

$$\langle \underset{\sim}{S} \rangle = - \frac{V_A}{4\pi} (B_{1\perp})^2 \cos\theta \hat{B}_0. \tag{7}$$

Alfvén waves can be classified on the basis of the number of dimensions in which $\underset{\sim}{B}_1$ fluctuates at an observing point, i.e., there are three-dimensional, two-dimensional, and one-dimensional Alfvén wave perturbations. Let us consider each type in turn.

1. Three-dimensional $\underset{\sim}{B}_1$ perturbations (General Alfvén Wave) In addition to properties 1.-4. above, a general Alfvén wave has the characteristics that

a. $|\underset{\sim}{B}| \equiv B = |\underset{\sim}{B}_0 + \underset{\sim}{B}_1|$ = constant.

b. $\underset{\sim}{B}_1$ moves in three dimensions.

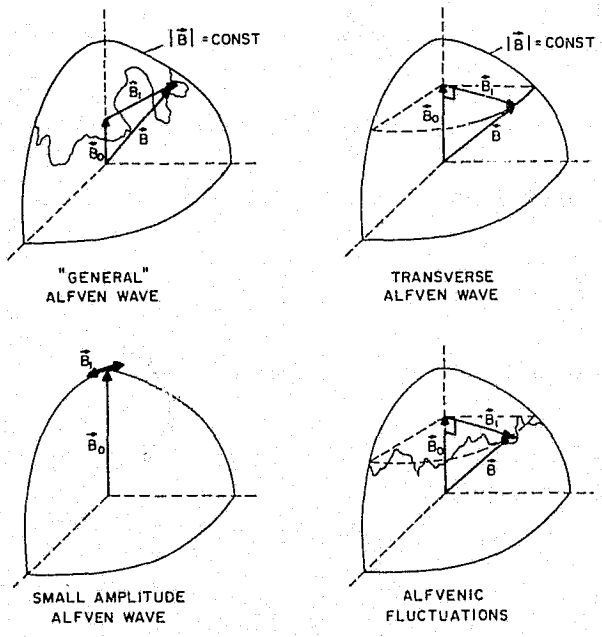


Fig. 1. Schematic depiction of the basic types of Alfvén waves (see Text). As shown, observed Alfvénic fluctuations combine features of both general and transverse fluctuations.

Thus, for this wave $B_{1\parallel} \neq 0$, and the tips of $\underset{\sim}{B}$ and $\underset{\sim}{B}_1$ move on the surface of a sphere (Figure 1a). That this type of Alfvén wave can exist has been demonstrated theoretically by Whang (1973), Goldstein et al. (1974), and Barnes (1974). The Poynting flux for this wave is given by Equation (5).

2. Two-dimensional $\underset{\sim}{B}_1$ perturbations (Transverse Alfvén Waves and Rotational Discontinuities) If $\underset{\sim}{B}_1(t)$ fluctuates in a plane, the locus of the tip of $\underset{\sim}{B}_1$ is a circle given by the intersection of this plane with the sphere $|\underset{\sim}{B}|$ = constant (Figure 1b). If the plane does not contain the center of the sphere, $\hat{B}_0$ may be defined as the direction normal to

the plane. Such Alfvén waves are called transverse Alfvén waves (TAW's) because $\underset{\sim}{B}_1$ is transverse to $\underset{\sim}{B}_o$ ($B_{1\parallel} = 0$). If the plane defined by $\underset{\sim}{B}_1$ does contain the center of the sphere $|\underset{\sim}{B}|$ = constant, then $B_1$ moves on the arc of a great circle of the sphere, $|\underset{\sim}{B}_1| = |\underset{\sim}{B}|$, and $\underset{\sim}{B}_o = 0$. If this case is regarded as the limiting case $B_o \to 0$, than $V_{Ao} \to 0$ and the Poynting flux goes to zero. This means that the "wave" does not propagate along $\hat{B}_o$.

For a TAW there is a minimum variance direction $\hat{m}$ of $\underset{\sim}{B}_1(t)$, which is parallel to $\hat{B}_o$ and thus defines $\hat{B}_o$. Clearly, $B_o = \underset{\sim}{B} \cdot \hat{m}$ and, of course, $\underset{\sim}{B}_{1\perp}$ = constant $\neq 0$ and $\underset{\sim}{B}_{1\parallel} = 0$. The minimum variance direction is determined by finding the direction $\hat{m}$ which minimizes $\langle[(\underset{\sim}{B} - \langle\underset{\sim}{B}\rangle)\cdot\hat{m}]^2\rangle$ (see Sonnerup, 1971; Burlaga and Turner*, 1976). This is equivalent to diagonalizing the matrix $\langle B_i B_j\rangle - \langle B_i\rangle\langle B_j\rangle$, i,j, = 1,2,3. The smallest eigenvalue, $\lambda_m$, is equal to the variance of $\underset{\sim}{B}$ along $\hat{m}$, i.e., $\lambda_m = \langle B_{1\parallel}{}^2\rangle$.

A rotational discontinuity is a special kind of transverse Alfvén wave with the characteristic that $\hat{B}_1$ changes discontinously in the MHD approximation. The wave moves along $\hat{B}_o = \hat{m}$, which is at an angle $\theta = \sin^{-1}(B_1/B_a)$ with respect to the ambient field $\underset{\sim}{B}_a$.

3. One-dimensional perturbations (small amplitude waves) If $\underset{\sim}{B}$ moves on an infinitesimal arc of the circle $|\underset{\sim}{B}|$ = constant, $\underset{\sim}{B}_1$ is parallel to the arc and is essentially along one dimension, say $\hat{p}$. Clearly this requires that $B_1 << \underset{\sim}{B}$ and it implies that $\hat{p}$ is normal to $\langle\underset{\sim}{B}\rangle$. One may choose $B_o = \langle\underset{\sim}{B}\rangle$, in which case $\langle\underset{\sim}{B}_1\rangle = 0$ (figure 1c). The average Poynting flux is $\langle\underset{\sim}{S}\rangle = \frac{V_A}{4\pi} B_1^2 \langle\hat{B}\rangle$. This wave has frequently been discussed in the literature of small amplitude MHD waves.

## 3. OBSERVED CHARACTERISTICS OF ALFVENIC FLUCTUATIONS

To the extent that the Alfvénic fluctuations observed in the solar wind resemble one or more of the Alfvén waves defined above, one can speak of the following wave characteristics:
(a) the correlation between $\underset{\sim}{V}_1$ and $\underset{\sim}{B}_1$; (b) the polarity; (c) the wave speed $V_{Ao}$; (d) the locus (dimensionality) of $\underset{\sim}{B}_1(t)$; and (e) the wave amplitude $B_1/B_o$. Two characteristics of AF's which are not consistent with the definition of an Alfvén wave are: (f) the existence of fluctuations in $|\underset{\sim}{B}|$, and (g) the presence of tangential discontinuities among AF's. It is also commonly assumed that AF's are plane waves, but it will be shown in section 4 that this is a questionable assumption.

We shall now consider in turn (a) through (g) above.

a. Correlation between $\underset{\sim}{V}_1$ and $\underset{\sim}{B}_1$. AF's have been studied in the time domain using both plasma and magnetic field data by Belcher, Davis and

Smith (1969) (BDS), Belcher and Davis (1971) (BD), Burlaga and Turner (1976) (BT), and Denskat and Burlaga (1977) (DB). Considering 6-hour intervals in the period June 14-Nov.21, 1967, BDS and BD found a correlation coefficient $\rho$ between $V_{1r}$ and $B_{1r}$ > 0.8 one third of the time. BD found $|\rho|$ > 0.6 55% of the time in that period. DB and BT considered one-hour intervals in periods during 1967, 1968 and 1971, and they found $|\rho|$ > 0.6 40% of the time. Thus, AF's represent a substantial fraction of interplanetary microscale fluctuations.

AF's have also been identified by Coleman (1966) using cross spectral analysis techniques. Considering fluctuations in the range 1 to 50 cycles per day for four 10-day periods and two 6-day periods, he found coherences between $V_r$ and $B_r$ of from 0.20 to 0.70, with an average of 0.46.

(b). Polarity The sign of the correlation coefficient or coherence between $\underset{\sim}{V}_1$ and $\underset{\sim}{B}_1$ indicates the direction of propagation of the wave. All of the authors quoted in (a) found that essentially all AF's are propagating away from the sun.

(c). Wave-speed The constant of proportionality between $\underset{\sim}{V}_1$ and $\underset{\sim}{B}_1$ is $K = V_{A_o}/B_o$ for an Alfvén wave. Thus, one can compare the "observed" $V_{A_o}$ with the "theoretical" value given by $V_{A_o} = B_o/\sqrt{4\pi\rho}$ by examining the distribution of $B_o K/(B_o\sqrt{4\pi\rho}) = K\sqrt{4\pi\rho} \equiv D$. This should be unity for an Alfvén wave, and indeed BDS, BT, and DB found $\langle D \rangle \simeq 1$. However, the distribution of D is broad, and values of D>2 are sometimes found; the reason for this is unknown.

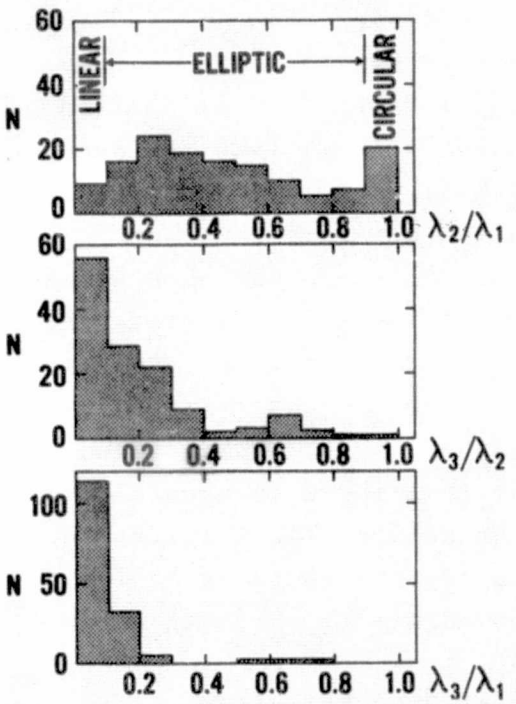


Fig. 2. Distributions of eigenvalues of the variance ellipsoids of $\underset{\sim}{B}$ for hour intervals relative to maximum eigenvalue $\lambda_1$, showing fluctuation close to but not entirely within a plane.

(d) Locus of $\hat{\underset{\sim}{B}}_1$ The distribution of $\hat{\underset{\sim}{B}}_1$ can be expressed as the distribution of the eigenvalue ratios $\lambda_3/\lambda_2$, $\lambda_2/\lambda_1$, $\lambda_3/\lambda_1$ which are obtained by diagonalizing the matrix $\langle B_i B_j \rangle - \langle B_i \rangle \langle B_j \rangle$. BDS observed that typically one eigenvalue was small and the other two larger and of comparable size, indicating that the magnetic field fluctuations were primarily in a plane, but they did not give the eigenvalue distributions. BD computed eigenvalues for the entire Mariner 5 data set, but they did not separate AF's from other fluctuations. BT and DB obtained the distributions, shown in Figure 2, of eigenvalues of AF's. $\lambda_3$ is the variance

of $\underset{\sim}{B}$ along $\hat{B}_0$, i.e., $\lambda_3 \equiv \langle B^2_{1\shortparallel} \rangle$. Figure 2 confirms the result of BDS, but it also indicates that $\lambda_3 \neq 0$. In particular, BT and DB found that $\langle B^2_{1\shortparallel} \rangle^{1/2} / \langle B^2_{1\perp} \rangle^{1/2} \lesssim (\lambda_3/\lambda_1)^{1/2} \simeq 0.1$. Taken literally, this means that there are non-zero fluctuations along $B_0$ and therefore that the fluctuations in B are 3-dimensional, i.e., the waves are general Alfvén waves. Nevertheless, it is true that the waves are nearly transverse (Figure 1c), and an error analysis has not been made to determine to what extent $\lambda_3$ is due to the small instrumental uncertainties. Figure 2 also shows that AF's are neither linearly polarized ($\lambda_2/\lambda_1 << 1$) nor circularly polarized ($B_1$ tracing a circle with $\lambda_2/\lambda_1 = 1$).

(e). Wave amplitude As noted by Hollweg (1978), there seems to be no distribution of $B_1/B_0$ for AF's in the literature. However, this ratio is probably close to 0.7 $\pm$ 0.1 based on studies by Chang and Nishida (1973) and BD, although those authors considered all types of fluctuations together, not just AF's. BT found a most probable value of between 0.3 and 0.4 for the relative amplitude of the transverse component of AF's.

Now we turn to two types of AF observations which are not consistent with the properties of Alfvén waves.

(f). Fluctuations in $|\underset{\sim}{B}|$ BD observed that small fluctuations in $|\underset{\sim}{B}|$ could be present among AF's. They found that in general $\langle B^2_{1\shortparallel} \rangle \lesssim 0.1 \langle B^2_{1\perp} \rangle$, and they concluded that Alfvén waves are dominant over compressive waves.

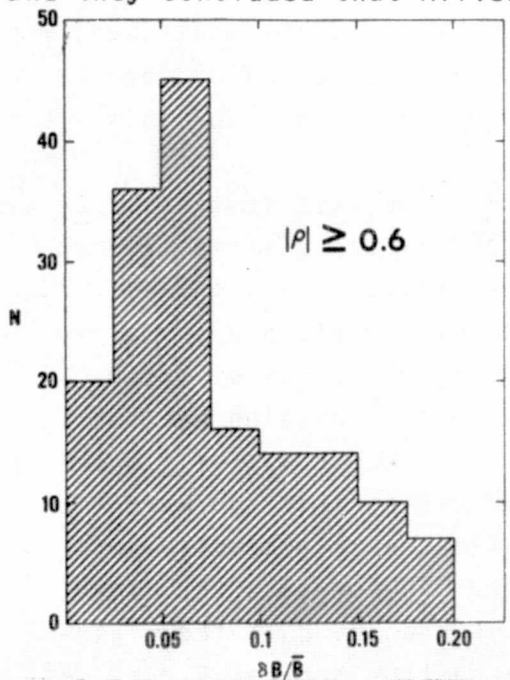


Fig. 3. Distribution of relative field magnitude fluctuations for events with $|\rho| \geq 0.6$ and $\delta B/\bar{B} < 0.2$. It is apparent that the fluctuations, though small, are not zero.

BT showed that in 85% of the AF's they examined, $\delta|\underset{\sim}{B}| \neq 0$. Their distribution of $\delta B/B$ (Figure 3) shows that the average is 0.06, which is at least six times greater than the experimental uncertainties. Thus, AF's are not pure Alfvén waves; they must include convected structures and/or compressive waves. Consistent with this are the observations of Sari and Behannon (1978) and Sari and Valley (1976) that there is generally a high coherency between fluctuations in $|\underset{\sim}{B}|$ and along $\langle \underset{\sim}{B} \rangle$ and those in at least one direction normal to $\langle \underset{\sim}{B} \rangle$ with phase of $0^o$ or $180^o$.

(g). Tangential Discontinuities among Alfvén Fluctuations The conditions for AF's are necessary but not sufficient conditions for Alfvén waves. There is no guarantee that a discontinuity across

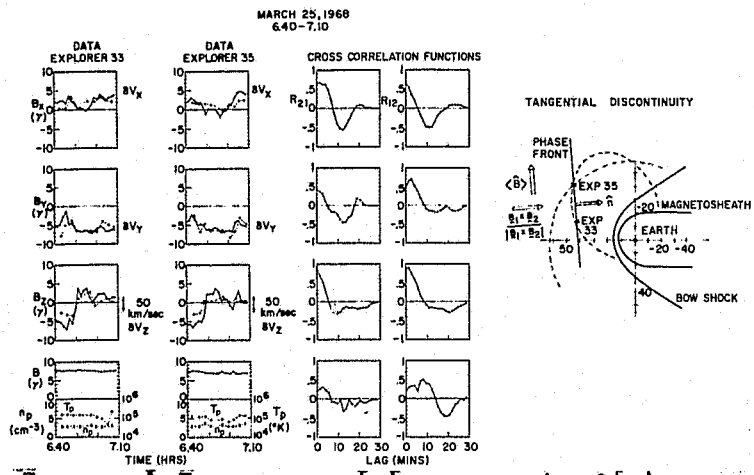


Fig.4. A TD observed in magnetic field and plasma data by both Exp.33 and Exp.35. Field is given in terms of solar ecliptic components and magnitude as solid lines; Solar wind speed, density and temperature as dashed lines. Cross-correlation functions were computed from magnetic field data.

which $\underset{\sim}{V}_1 \approx (V_{A_0}/B_0)\ \underset{\sim}{B}_1$ is an RD, for example. DB showed examples of TD's among AF's (Figure 4); The TD's were identified by determining the orientation of the discontinuity surface from the time delay in moving from one spacecraft to another, and then by showing that there was no component of $\underset{\sim}{B}$ along the normal to that surface. Burlaga et al. (1978) have also demonstrated that TD's can exist among AF's. They identified the TD's by means of a minimum variance analysis of the current sheets associated with the discontinuities. The occurrence of convected structures among AF's might simply be the result of Alfvén waves moving through an ensemble of stationary structures.

## 4. ARE ALFVENIC FLUCTUATIONS PLANE WAVES?

It is usually assumed that "Alfvén waves" in the solar wind are plane waves. This means that $\underset{\sim}{B}_1$ and $\underset{\sim}{V}_1$ are functions of $x-V_A t$, where $\hat{x}$ is the direction of propagation. The amplitude, $B_1$, and the propagation vector, $\hat{k}$, of a plane wave are the same everywhere in the (y,z) plane. Thus a spacecraft which intercepts a phase plane at one point should measure the same amplitude and $\hat{k}$ as a second spacecraft which intercepts the phase plane at any other point. In other words, two spacecraft separated by any distance $\underset{\sim}{L}$ should measure the same $\underset{\sim}{B}(t)$ profiles (except for a phase difference) and the same $\hat{k}$. Obviously, truly plane waves do not exist. The relevant question is "over what distances are AF's approximately planar in the solar wind?". This question cannot be answered with observations from just one spacecraft.

Given observations of Alfvénic fluctuations from 2 spacecraft separated by a distance L, one can test for planarity of the waves (1) by comparing $\hat{k}_1$, measured locally at spacecraft 1 with $\hat{k}_2$ measured locally at spacecraft 2, or (2) by comparing $\hat{k}$ measured locally at one spacecraft with the phase plane normal, $\hat{n}$, calculated on the assumption that the wave is a plane wave. If the fluctuations are plane waves, one should

find that $\hat{k}_1 = \hat{k}_2$ and that $\hat{k}_{1,2} = \hat{n}$. For transverse waves one should have that $\hat{k} = \hat{m}$, and $\hat{n}$ can be calculated by a geometrical argument which uses the phase lag of $\underset{\sim}{\delta B}$ (t) between the two spacecraft and the measurements of solar wind velocity. Actually, with 2 spacecraft in the ecliptic plane, only the projection of $\hat{n}$ in the ecliptic plane, $\hat{n}_p$, can be determined. This must be compared with the corresponding component of $\hat{k}$, i.e., with $\hat{k}_p$, in testing for planarity.

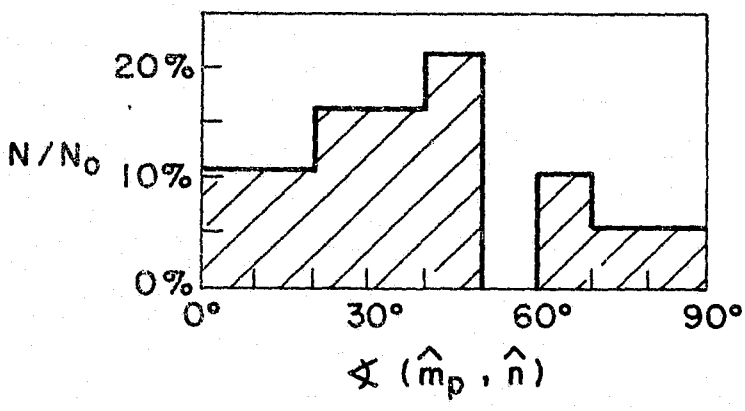


Fig. 5. Distribution of the angle between the eigenvector $\hat{m}_p$, corresponding to the minimum variance direction projected into the ecliptic plane, and the wave vector $\hat{n}$ for propagating plane wave fluctuations.

This latter method was used by DB. They tested for the planarity of AF's observed in 1-hour intervals by 2 spacecraft separated by 20-70 $R_E$. Their result is shown in Figure 5. This illustrates that, in general, for 17 cases $\hat{n}_p$ was not parallel to $\hat{k}_p$. Thus the AF's observed were apparently not plane over distances of 20-70 $R_E$. Since DB were only able to test 17 one-hour intervals, it is not known whether their results are truly representative of all AF's in the solar wind.

## 5. PROPAGATION OF ALFVENIC FLUCTUATIONS

Assuming nearly plane waves and using geometric optics, Barnes (1969) and Völk and Alpers (1973) predicted that the wave vector $\hat{k}$ for MHD waves would be refracted as the waves propagate such that $\hat{k}$ is essentially radial at 1 AU if it has started out parallel to $\underset{\sim}{B}_0$ near the sun. This is in the absence of velocity gradients, however, i.e., it is based on a simple model of symmetric radial flow. When the velocity gradients in streams are also considered, as has been done by Barnes and Hollweg (1974), Hollweg (1975), Richter and Olbers (1974) and Richter (1975), then, rather than being radially directed at 1 AU, the wave vector $\hat{k}$ is refracted westward (away from $B_0$) at the front of a stream and eastward (toward $B_0$) at the rear of the stream.

For plane transverse Alfvên waves, the wave normal is given by the minimum variance direction. Analysis of AF's show that the minimum variance direction is usually close to the mean field direction rather than in the radial direction (BDS, BD, DB). Solodyna and Belcher (1976),

Burlaga and Turner (1976) and Daily (1973) showed that this is true also for both compression and rarefaction regions of streams. Thus, the observed minimum variance directions do not agree with the directions of wave normals predicted by the theories.

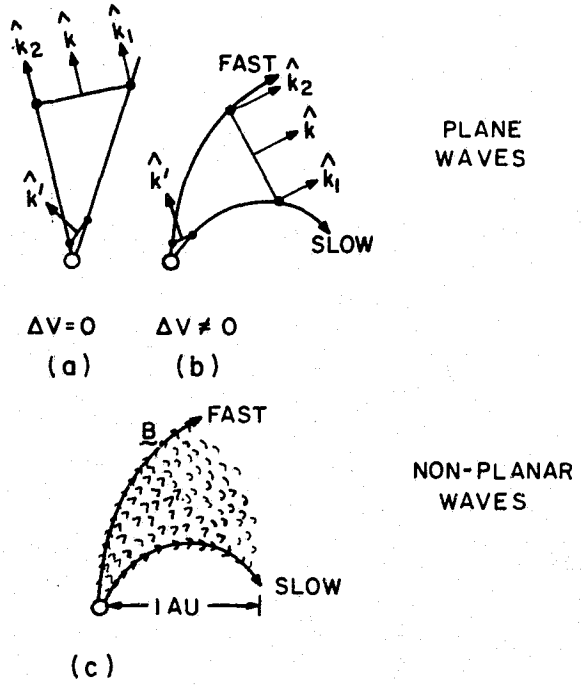


Fig. 6. Illustration of (a) plane wave propagation without gradients, (b) plane wave propagation with stream effects included, and (c) propagation of waves appreciably curved on a scale $\lesssim$ 0.01 AU.

The theoretical predictions are all based on the assumption that the waves are plane over distances on the order of $\sim$1 AU, as illustrated in Figure 6. The tendency for $\hat{k}$ to become radial in the absence of gradients is the geometrical effect shown in Figure 6a. When streams are included, the gradients produce the deflections illustrated by the sketch in Figure 6b, mainly by convection. The various arguments do not apply, however, if the waves are not plane waves over distances on the order of the scale of streams and stream gradients. In particular, they are inapplicable if the waves are curved appreciably on a scale of $\lesssim$ 0.01 AU, as shown in Figure 6c. For waves that are not plane waves, $\lambda_{min}$ can always be close to $\langle \underset{\sim}{B} \rangle$ and still be variable over distances > 0.01 AU because $\langle \underset{\sim}{B} \rangle$ itself is variable over such distances. The fact that the autocorrelation length of $\underset{\sim}{B}$ is $\approx$ 0.01 AU is consistent with this picture.

## 6. STABILITY OF ALFVÉNIC FLUCTUATIONS

The stability of Alfvén waves in the limit $\beta \equiv nkT/(B^2/8\pi) \to 0$ has been investigated theoretically by several authors (Galeev and Oraevskii, 1969; Hollweg, 1971; Cohen and Dewar, 1974; Cohen, 1975; Chin and Wentzel, 1972; Lashmore-Davies, 1976). Although several types of instabilities have been identified, the assumption $\beta \to 0$ is not applicable to the solar wind, so it is not certain that those instabilities can occur in the solar wind.

Recently Goldstein (1978) has investigated the stability of a finite-amplitude, circularly-polarized Alfvén wave for the case $\beta \lesssim 1$, which is the relevant case for the solar wind. He found that the waves can decay

for all $\beta<1$ by means of an MHD modulational instability. In particular, an Alfvén wave decays into a forward-propagating magnetic wave, a forward-propagating density wave, and a backward-propagating magnetic wave. The decay waves are not normal modes of the plasma. The decay occurs as a result of the Alfvén wave coupling to random density and magnetic fluctuations in the ambient medium. The growth rate of the driven waves increases with $\delta|B|/B$ and decreases with increasing $\beta$. It is surprisingly large in general. The decay of AF's may be an important factor in heating and accelerating the solar wind.

The growth of Alfvén waves as a result of an instability produced by the velocity shear in streams has been investigated by Bavassano et al. (1978). They have found that short wavelength waves moving in a direction close to that of the mean magnetic field can grow in velocity shear regions under the conditions observed near 1 AU, and they observed magnetic field fluctuations in such regions which are consistent with those predicted by the theory. They also have concluded, however, that most of the long wavelength Alfvén waves could not be produced in this way, and hence that they probably originate near the sun.

## 7. SUMMARY AND CONCLUSIONS

Results obtained during the last few years have confirmed that fluctuations in the bulk velocity of the solar wind are correlated with fluctuations in the magnetic field more than one-third of the time and that these Alfvénic fluctuations have several characteristics in common with Alfvén waves. However, it has also been shown that AF's are not "pure" Alfvén waves, because there are fluctuations in magnetic intensity and because tangential discontinuities can be found among AF's. Furthermore, there is evidence that the plane wave assumption used in most theoretical studies of Alfvén wave propagation is not valid over distances $> 0.01$ AU.

Several important questions have been raised and should guide further studies of AF's. These include the following. What is the cause of the variations in magnetic field intensity in AF's? Over what distances are AF's approximately plane waves, and how does this change with interplanetary conditions? Is there a turbulent cascade of energy or simple mode-coupling near 1 AU? Are AF's general Alfvén waves? The answers to these questions will require accurate, simultaneous plasma and magnetic field data from at least two spacecraft with separations in the range $< 50{,}000$ km to $> 500{,}000$ km. Also needed is a better theoretical understanding of the behavior of large amplitude Alfvén waves, especially

with respect to their coupling to other modes, their stability, and their propagation. A kinetic theory approach to these problems is particularly needed.

## 8. REFERENCES


Barnes, A., Collisionless heating of the solar wind plasma. 2. Applications of the theory of plasma heating by hydromagnetic waves, Astrophys.J., 155, 311, 1969.

Barnes, A., Theoretical studies of the large-scale behavior of the solar wind, Advan.Electron. Electron Phys., 36, 1, 1974.

Barnes, A., Hydromagnetic waves and turbulence in the solar wind, in Solar System Plasma Physics, ed. C.F. Kennel, L.J. Lanzerotti, and E.N. Parker, North-Holland Publishing Co., 1978.

Barnes, A., and J.V. Hollweg, Large-amplitude hydromagnetic waves, J.Geophys.Res., 79, 2302, 1974.

Bavassano, B., M Dobrowolny, and G. Moreno, Local instabilities of Alfvén waves in high speed streams, Solar Phys., 57, 455, 1978.

Belcher, J.W., and L. Davis, Jr., Large-amplitude Alfvén waves in the interplanetary medium, 2, J.Geophys.Res., 76, 3534, 1971.

Belcher, J.W., L. Davis, Jr., and E.J. Smith, Large-amplitude Alfvén waves in the interplanetary medium: Mariner 5, J.Geophys.Res., 74, 2302, 1969.

Burlaga, L.F., and J.M. Turner, Microscale "Alfvén waves" in the solar wind at 1 AU, J.Geophys.Res., 81, 73, 1976.

Burlaga, L.F., J.F. Lemaire, and J.M. Turner, Interplanetary current sheets at 1 AU, J.Geophys.Res., 82, 3191, 1977.

Chang, S.C., and A. Nishida, Spatial structure of transverse oscillations in the interplanetary magnetic field, Astrophys. Space Sci., 23, 301, 1973.

Chin, Y.C., and D.G. Wentzel, Nonlinear dissipation of Alfvén waves, Astrophys. Space Sci., 16, 465, 1972.

Cohen, R.H., Mode decay and evolution of the solar wind Alfvén wave spectrum, J.Geophys.Res., 80, 3678, 1975.

Cohen, R.H., and R.L. Dewar, On the backscatter instability of solar wind Alfvén waves, J.Geophys.Res., 79, 4174, 1974.

Coleman, P.J., Jr., Hydromagnetic waves in the interplanetary plasma, Phys.Rev.Lett., 17, 207, 1966.

Daily, W.D., Alfvén wave refraction by interplanetary inhomogeneities, J.Geophys.Res., 78, 2043, 1973.

Denskat, K.U., and L.F. Burlaga, Multispacecraft observations of microscale fluctuations in the solar wind, J.Geophys.Res., 82, 2693, 1977.

Galeev, A.A., and V.N. Oraevskii, Dokl.Akad.Nauk,SSR, 147, 71, 1962 (Sov.Phys.Dokl., 7, 988, 1963).

Goldstein, M.L., An instability of finite amplitude circularly polarized Alfvén waves, to appear, Astrophys.J., 1978.

Goldstein, M.L., A.J. Klimas, and F.D. Barish, On the theory of large-amplitude Alfvén waves, in Solar Wind Three, ed. C.T. Russell, p. 385, U. California Press, Los Angeles, 1974.

Hollweg, J.V., Nonlinear Landau damping of Alfvén waves, Phys.Rev.Lett., 27, 1349, 1971.

Hollweg, J.V., Hydromagnetic waves in interplanetary space, Publ. Astron. Soc. Pac., 86, 561, 1974.

Hollweg, J.V., Waves and instabilities in the solar wind, Rev.Geophys. Space Phys., 13, 263, 1975.

Hollweg, J.V., Some physical processes in the solar wind, to appear, Rev. Geophys. Space Phys., 1978.

Lashmore-Davies, C.N., Modulational instability of a finite amplitude Alfvēn wave, Phys.Fluids, 19, 587, 1976.
Richter, A.K., Wave-trains in the solar wind. III: Alfvēn waves in the azimuthally-dependent interplanetary medium, Astrophys.Space Sci., 36, 383, 1975.
Richter, A.K., and D.J. Olbers, Wave trains in the solar wind. 2. comments on the propagation of Alfvēn waves in the quiet interplanetary medium, Astrophys.Space Sci., 26, 95, 1974.
Sari, J.W., and K.W. Behannon, The existence of finite amplitude, nonplanar Alfvēn waves in the interplanetary medium, preprint, 1978.
Sari, J.W., and G.C. Valley, Interplanetary magnetic field power spectra: mean field radial or perpendicular to radial, J.Geophys.Res., 81, 5489, 1976.
Solodyna, C.V., and J.W. Belcher, On the minimum variance direction of magnetic field fluctuations in the azimuthal velocity structure of the solar wind, Geophys.Res.Lett., 3, 565, 1976.
Sonnerup, B.U.Ö, Magnetopause structure during the magnetic storm of September 24, 1961, J.Geophys.Res., 76, 6717, 1971.
völk, H.J., Microstructure in the solar wind, Space Sci. Rev., 17, 255, 1975.
Völk, H.J., and W. Alpers, The propagation of Alfvēn waves and their directional anisotropy in the solar wind, Astrophys.Space Sci., 20. 267, 1973.
Whang, Y.C., Alfvēn waves in spiral interplanetary field, J.Geophys.Res., 78, 7221, 1973.

# LOCAL AND GLOBAL PROCESSES WHICH IMPACT SOLAR WIND ELECTRONS

J. D. Scudder
NASA/Goddard Space Flight Center
Laboratory for Extraterrestrial Physics
Greenbelt, Maryland 20771 USA
and
S. Olbert
Massachusetts Institute of Technology
Department of Physics and
Center for Space Research
Cambridge, Massachusetts 02139 USA

ABSTRACT A new detailed first principle kinetic theory for solar wind electrons which is neither fluid nor exospheric in nature is presented. This theory illustrates the global and local properties of the solar wind expansion and coulomb collisions that are reflected in the observed electron velocity distribution function--such as its bifurcation, skewness, and the "differential" temperatures of the thermal and suprathermal subpopulations. This theory is also shown to make numerous predictions of correlations amongst electron solar wind parameters which have been previously reported.

The extant models of the solar wind represent the extremes of approximations that can be made using the Knudsen number ($K = \lambda_{mfp}/H$) as an ordering parameter: the fluid approximation ($K \ll 1$) enjoys a certain popularity because of its tractable mathematics, although the transport coefficients (such as the thermal conductivity, viscosity, etc.) that are used seem dubious at best (c.f., Kopp and Orrall, 1977, for a recent review); the exospheric approach ($K \sim \infty$) is hampered by the non-uniqueness of the solutions which satisfy the Vlasov equation. Direct observations (Ogilvie and Scudder, 1978) indicate that reality at 1 AU for electrons is in between these two extremes with $K_e \sim 1$. This paper discusses the first quantitative attempt to discuss the physics of solar wind electrons in the more realistic, intermediate Knudsen number regime.

The electron Knudsen number at 1 AU is comparable to that expected in the acceleration regime of the solar wind in the lower corona. If we can understand what factor(s) control the observed heat flow, it seems likely that this understanding could impact the current reexamination of the solar wind energy budget in the acceleration regime. We begin our discussion with a brief overview of *in situ* observations of

electrons at 1 AU which provide yardsticks for assessing theoretical attempts to understand solar wind electrons.

The low energy thermal portion of the electron velocity distribution function has been called the "core" or "cold" component and approximates, with some license a paraboloid in ln(f) vs velocity; the suprathermal component (i.e., everything which is not the core) is often called the "halo" or "hot" component. There is some effective Maxwellian with a "differential" temperature which approximates these populations. The effective "temperature" of the suprathermal component is substantially larger than that of the thermal component; its "density" is only a few percent of the ion charge density. The signature that this distribution is carrying a heat flux is the asymmetry of this distribution function. The electrons that are carrying the heat are not those as in small Knudsen number transport theory where there is a slight skewness in f(v) in the vicinity of one thermal speed; these asymetries are observed at higher speeds (usually above 2-4 (rms) thermal speeds, and $f_{observed}$ cannot be represented by a single Maxwellian.

A brief list of observed interrelationships of solar wind electrons is given below. The halo density fraction of the total density is nearly independent of large variations in the ambient density. This number turns out to be on the order of $6\pm2\%$ (where we have used deviations quoted by Feldman et al., 1975). The ratio of the suprathermal to thermal "temperatures" is remarkably constant with a value something like $6\pm1$. The halo fraction of the total density is strongly anti-correlated with the local bulk speed (if it is nearly the asymptotic bulk speeds, Scudder and Olbert (1978a)). The differential temperature of the halo population is anti-correlated with the bulk speed; and the heat flux is lower in absolute magnitude in high speed wind than in the low speed wind (Feldman et al., 1976 and Rosenbauer et al., 1977).

A further point of some interest concerns the reproducibly bi-model appearance of the electron distribution function. If we plot ln(f) vs proper frame kinetic energy for particles moving both along and opposed to the local magnetic field direction, there is a break energy, E*, between approximately linear segments, which empirically scales as $E^* = 7kT_c$ (Scudder and Olbert, 1978b). This energy has an

intrinsic relation to the properties of Coulomb collision cross section and its velocity dependence.

The radial variations of the core and the halo components have been determined from data returned by the Plasma Science Experiment on Mariner 10 (Ogilvie and Scudder, 1978). The radial variation of the core electron temperature between 0.4 and 0.85 AU was approximated as an inverse power law with exponent $0.3 \pm 0.08$ and that of the halo component was essentially without radial variation. If we extrapolate these radial dependences toward the sun we obtain some indication that there is a common zone where these particles may have previously been members of the same Maxwellian population above and below the break point energy, $E^*$. This radial position where the two radial profiles converge is in the proximity of $2\text{-}15 R_\odot$.

In Figure 1a we show data acquired by the NASA/GSFC VES instrument on ISEE-1 in the format (ln(f) vs $w_{\parallel}$). The characteristic low energy thermal component and the characteristic break point energy are clearly shown; the kinetic information in this figure is immediate: the system is not in local thermodynamic equilibrium (LTE)--if it were in LTE with the same internal energy it would look in this format as in figure 1b. Immediately we can state that the Braginskii (1965) (small Knudsen number) formulae for transport coefficients are not relevant for this system; Fourier's law ($Q = -\kappa \nabla T$) does not apply in most of the relevant regimes of the solar wind. Fourier's law is a gross oversimplification of the physics of heat transport in an inhomogeneous plasma and only obtains theoretically under extremely simplifying assumptions. We must attempt a kinetic type formulation, in the presence of Coulomb collision and $K_e \sim 1$; we have to compute the electron distribution function both in configuration and velocity

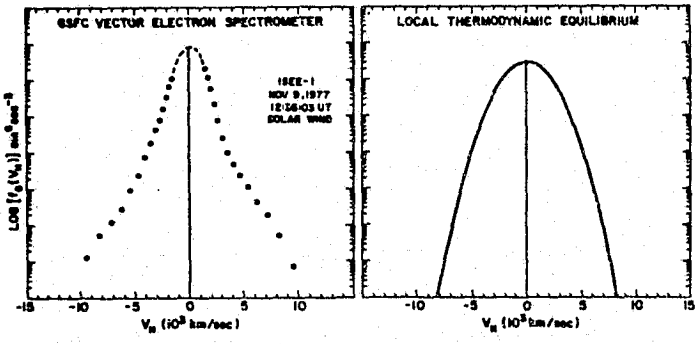


FIG. 1a FIG. 1b

space. We then have to take the appropriate moment of the distribution function to determine the flow of heat. Clearly, if we have a theory which can replicate the observation of the distribution function, then we may have some hope in developing a quantitative discussion of the flow of heat in this system.

The Coulomb interaction between a "test" electron and the plasma is often broken up into regimes for which the test electron has an impact parameter, b, less than and greater than the shielding debye length, $\lambda_d$, (c.f., e.g., Cohen et al., 1950 or Krall and Trivelpiece (1973)). The interactions with $b < \lambda_d$ may be visualized as binary in character with shielded ion scattering sites; when $b > \lambda_d$ the interaction is a many body interaction of the test particle with the correlations of the targets on a scale $L > \lambda_D$ and is a "wave-particle" interaction.

In this paper we will discuss the strict consequences of (binary) Coulomb collisions in the cavity occupied by the solar wind. Our considerations will give rise to a global sense of causality, whereby we shall come to understand that the in situ electron observations are connected in rather dramatic ways to the extremities of the heliospheric cavity. This, in turn, implies that to interpret the local observation of the electrons in the medium, one must be thinking about the system in the large.

Our approach is to start from the Boltzmann equation with a relaxation time approximation for the Coulomb scattering operator. The relaxation time approximation is also known as the Krook approximation (Gross and Krook (1956)) and is currently being used as a mathematical simplification to see qualitative effects; the information obtained is already sufficiently instructive to illustrate interesting features of a fully ionized plasma which is inhomogeneous. The relaxation time scale we have used is the velocity dependent Coulomb time scale for an effective $90^o$ deflection; the explicit formulae are discussed in detail in Scudder and Olbert (1978a). The approach is to discuss an approach via perturbation where a guess motivated from observation, for the equilibrium spatial profile, $F(\underline{r},\underline{v})$, is assumed to be a convected Maxwellian with a specified radial dependence of density, thermal (core) temperature and bulk speed. We then inquire, via the relaxation approach, "how do the local Maxwellian populations

'accommodate' or take notice of their environment as allowed by the smooth forces and Coulomb scattering that the electrons experience, enroute to setting up a microscale consistent with the macroscale forces and the properties of Coulomb collisions?" The empirically motivated choice of a local Maxwellian stems from the evidence at all radii for which direct observations have been made that there is an approximately Maxwellian core or cold component for the electron distribution function. Direct in situ determinations (Ogilvie and Scudder, (1978)) of the mean free path for Coulomb collisions over the scale height indicate that there are marginally enough Coulomb collisions to start the process of local Mawellization.

Formal solutions to the Boltzmann partial differential equation are rarely of much help in calculating the solution, but they often provide valuable qualitative insights into the physical processes at hand. The formal steady state solution for our problem at a given time, $t^*$, at a given location, $r^*$, and at a given velocity $\underline{v}$, is given by

$$f(\underline{v}^*,\underline{r}^*,t^*)=F(\underline{v}_o,\underline{r}_o)\exp(-S_o)+\int_{t'}^{t^*}\exp(-S(\underline{r}',\underline{v}',\underline{r}^*,\underline{v}^*,t^*))F(\underline{v}',\underline{r}')/\tau[t']\,dt' \qquad (1)$$

where $$S(\underline{r}',\underline{v}',\underline{r}^*,\underline{v}^*,t^*)\equiv\int 1/\tau[t'']\,dt''.$$

The structure of this solution is particularly interesting since it illustrates the global nature of the eventual solutions we will obtain. The first term represents an attenuated, $\exp(-S_o)$, signal of "source" phase density from the boundary; the additional term represents the superposition of "source" phase density which can reach the observer from intervening spatial layers properly attenuated for the intervening depth, $S(r',r^*)$. Let's examine the nature of this quantity S in the formal solution. The quantity S is a counter of the effective number of Coulomb collisions experienced by a representative element in the phase space going along the characteristic in the presence of the smooth forces from $(r',t')$ to $(r^*,t^*)$. The quantity $\exp(-S)$ which occurs in the formal solution is also a very interesting quantity to understand. This quantity is the normalized survival probability to transit from $(r',t')$ to $(r^*,t^*)$ without experiencing an effective $90^o$ coulomb scattering. The equations of motion are hidden

in this formal solution; the attenuation provided by the Coulomb effect is explicitly present in the S quantity. The extinction provided by the Coulomb scattering is analogous to the similar behavior of the optical depth ($\tau(\nu)$) of radiative transfer theory; we will refer to this quantity S as the "collisional depth".

If we consider an observer at 1AU it is important to know how large S is as a function of energy. This quantity can be shown a posteriori to range from approximately 2 to over 30 when one considers electrons with local kinetic energy at 1AU which range from 500eV to 5eV. This immediately implies that in the solar wind we are connected in a dramatic way at higher energies to the plasma microstate in vicinities well removed from that of the place of observation, since the observer is not screened off from large phase densities at this boundary at this energy. This implies that for any physical quantity which depends on the moderate to higher energy electrons, such as the heat flux, one must consider the entire system. Because of this global connectivity local Knudsen number arguments appear inadequate to vindicate Fourier's law in inhomogeneous plasmas. This is not the whole story -- this is just the extinction portion of the contributions to the local phase density; there remains the question of the energetic accessibility.

We have seen that this quantity exp(-S) is a normalized survival probability. Can we understand microscopically from the properties of Coulomb collisions , what allows this "transparency" of the corona to the observer? In Figure 2 we illustrate a universal plot of the properties of a fully ionized plasma for which $T_e << (m_p/m_e)T_p$. The ordinate is exp(-S) and the abscissa is the scaled quantity $u = w/w_{T_e}$, where w is the electron's proper frame speed and the normalizing factor for u is the rms thermal speed of the electrons. We have asked

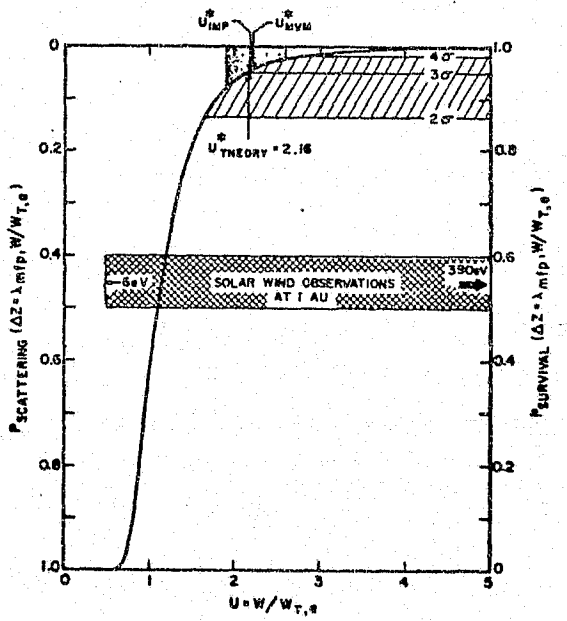


FIG. 2

the question "what is the survival probability for traversing a fiducial local length in the plasma, namely the local free path for the rms thermal electron, as a function of test electron speed?" Because u is a scaled dimensionless quantity, this is an universal plot for the above stated temperature range. We now ask what is a reasonable statistical definition that a test electron "survives" without having an effective $90^{o}$ scattering while transiting this fiducial length. Since this is a statistical question a customary level of confidence is 3 sigma. If we adopt this level of certainty we define a characteristic scaled speed $u^{*}=2.16$. If we also recognize that this is a statistical relation, then we should expect some dispersion in this quantity, say, ranging from 2-4 sigmas. For particles above this range of characteristic speeds, we thus argue that these particles last Coulomb scattered more than one local rms thermal speed electron's free path away from the observer. In principle we have established that there is a collisional window above this speed range to whatever plasma populations are beyond our fiducial length. If we examine breakpoint data from experimental data from all the Mariner 10 data and an analysis of published IMP data we obtain the most probable points for u* as indicated on the figure. These most probable experimental points nearly coincide with the quantity $u^{*}$. The entire range of experimental values of the breakpoint energy determined on Mariner 10 is indicated by the stippled zone on this figure. This zone is centered in the 2-4 sigma zone defined previously. This spread is also consistent with the uncertainties in a re-analysis of published IMP data (Scudder and Olbert, 1978b). This is a very strong argument in our opinion that Coulomb processes may be the dominant factor in determining the local distribution function. This also means that Coulomb physics is also intrinsic to the conduction problem since the break point energy is in the proximity of the largest skews of the local distribution function.

If we are going to integrate the Boltzmann equation we must think seriously about the smooth forces which the electrons experience enroute to the observer. This raises the question of what are the smooth forces which the electrons experience? Among the most important smooth forces is the parallel electric field which the charged particles experience because the medium is inhomogeneous. This parallel electric field is present in all fluid theories which impose the external condition that the medium be pointwise neutral and that the electron and ions have the same bulk speeds. This parallel

electric field can be determined from the generalized Ohm's law (c.f. Scudder and Olbert, 1978a for details), once the electron pressure and density variation have been given (as in our initial ansatz, supra). Our polarization potential barrier is very similar to that published by Lemaire and Scherer, 1973). This potential represents a significant barrier of the order of 1.5 keV to the progress of electrons along the tubes of force from the corona (we have assumed a Parker spiral). This is especially critical since the electrons observed at earth presumably originate in a thermal plasma in the corona with a kT of the order of 100eV.

If we return to the formalism, we can see by integration by parts that (1) may be rewritten as a superposition of two terms

$$f(t) = \underset{\text{(Local)}}{F(\Delta S = 0)} + \underset{F(\Delta S = 0)}{\overset{F(\Delta S = S_o)}{\oint}} \exp\left(-\Delta S\left(F[t(\Delta S)]\right)\right) dF \qquad (2)$$

(Global)

one that is by definition local, ($\Delta S=0$), plus a superpositon of differential phase density that is accessible to the observer multiplied by the probability that it does not get extincted enroute to the observer. We see immediately that the departure from the local distribution function is this global integral. Since there appears, by direct observation, to be a marginally adequate number of collisions to Maxwellize the low energy "core" we see from (2) that taking F to be the local Maxwellian is a good idea. Among the details required to "realize" a solution of the Boltzmann problem, one must collect all contributions (in steady state) which could have ever made it to the observer. In this connection it is important to notice that in the entire solar system it is very difficult to get electrons to cross magnetic tubes of force, either by finite radii effects or collisional diffusion. (This means the life and death of the electron is along the same field line upon which it was injected in the lower corona. This means that the problem is topologically one dimensional). This implies that the stochastic problem of getting all the contributions is restricted to the given tube of force which the threads the position of the observer. The contributions from a given layer at r' can contribute particles going both fore (away from sun) $f^{+}(+\underline{v}^{*},\underline{r}^{*})$ and aft $f^{-}(-\underline{v}^{*},\underline{r}^{*})$ along the local magnetic field at the observer; conversely the observer measuring $f^{+}(\underline{v}^{*},\underline{r}^{*})$ will in general have non-negligible contributions from radial positions along the tube

of force that are both inside and outside that of the observer. It is quite possible on the basis of kinematic accessibility that the electrons which comprise the local aft halo phase density, $f^-$, originated in the corona, propagated along the local tube of force, passed the location of the observer at some earlier time, proceeded along the tube of force and have been scattered back toward the site where they come to be observed going toward the sun. This same level in the corona can also contribute strongly to the forward portion of the halo $f^+$. Clearly, in steady state there is also the kinematic possibility that there are more than one turning point orbits between "source" layers and the observer; the problem of getting all the contributions comes down to tracking down all these turning point orbits. Due to the limitations of space in the present monograph we will not pursue this details as they are available in the literature (Scudder and Olbert, 1978a).

Another example of the electron distribution function is given in Figure 3 where we have plotted the distribution function in the proper frame adapted from Feldman et al., 1975, as discussed in Scudder and Olbert (1978a). The principle reason for this figure is to show that different experimental groups obtain similar velocity distributions (compare figure 1a) and establish a basis for comparison with the theoretical realizations which we will subsequently discuss. The thermal and suprathermal populations are clearly present; the break between the two parabolas occurs at approximately 2 rms thermal speeds; the break in the profiles occurs roughly two and one-half orders of magnitude below the maximum value of the entire distribution function; the distribution is skewed with a magnitude which should be

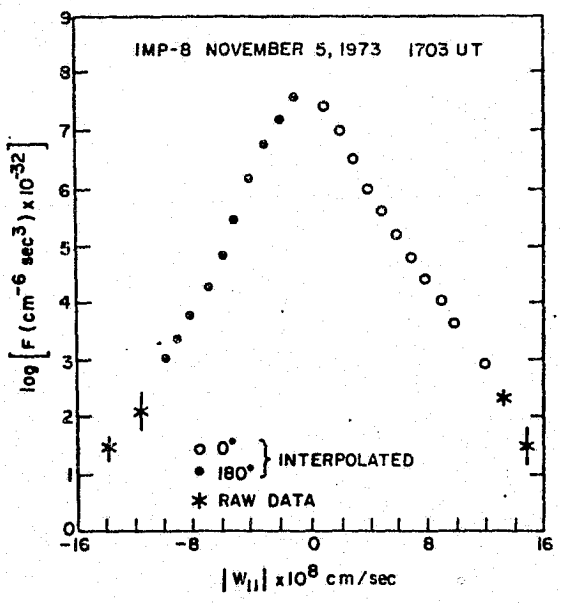


FIG. 3

compared with the theoretical solutions; the ratio of the fore and aft phase density $f^{+}/f^{-}$ asymptotes to a value of approximately 6.

Figure 4 shows a plot in the same format as that of Figure 3 of a theoretical solution with an asymptotic solar wind speed of 400km/s. The logarithmically spaced dots are the theoretical solution; the parabola is the local Maxwellian ansatz, $F = f^{(o)}_{k}$. Among the features of this profile are the suprathermal population, present even though no wave particle interactions were included in this theory, the suprathermal population with approximately the correct relative importance in the overall distribution function, the skewness of the distribution function, which compares favorably with that illustrated in the previous figure of in situ data, the bifurcation of the distribution function, and the break point energy of the solution which automatically has the correct position since this is an intrinsic property of the Coulomb scattering process.

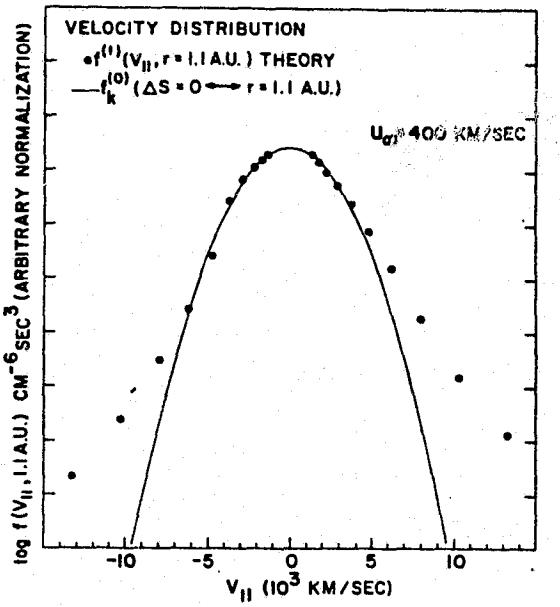


FIG. 4

From this solution we will establish contact with the experimental extrapolation of the radial variation of the core and halo being consistent with a prior contact at different times with the same Maxwellian population somewhere in the regime of 2-15 $R_o$. Let's ask, "where were the collected electrons last members of a Maxwellian

'source' population?" We consider in Figure 5 these radial source regions. The vertical axis is the contribution of phase density which is ultimately collected at the indicated observer's position and the horizontal axis is the radial location of the Maxwellian from which the contribution comes. The 5eV electrons collected at 1AU are seen to have come most recently from a Maxwellian population in the immediate proximity of the observer; $f^+$(5eV) comes predominately from a Maxwellian population inside the radial position of the observer; $f^-$(5eV) comes from slightly outside the observer. Both these contributions are from within one rms thermal free path of the observer. By contrast, consider the radial positions of the dominant contribution of the phase density for kinetic energy 500eV at 1AU. We see that both $f^+$ and $f^-$ contributions at 1AU originate in collisional populations very near the base of the corona in the region of 1-10$R_\odot$. We thus see that we recover (by considering the Coulomb extinction and the self consistent forces) the experimentally inferred regime of common thermal origin, since the thermal core has been reprocessed many times in different collisional populations with different T's. There is little doubt that at an earlier time the thermal electrons were in collisional equilibrium with other electrons near the base of the corona.

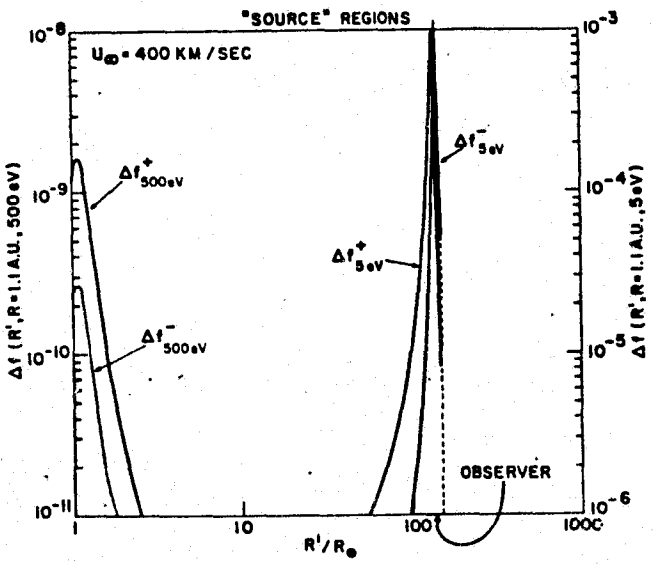


FIG. 5

This figure also dramatically illustrates the direct contact which the 1AU observer has (at suprathermal kinetic energies) to the boundaries of the system. In these senses the in situ electron distribution function has both local and global information in it: the thermal regime has the local gradient physics; the population of the $f^+$ in the suprathermal regime proclaims the existence of the hot, very dense

corona many mean free paths away- and the skewness of the superathermals contains the information of the transit of these particles beyond the observer in the distant heliosphere where they are backscattered to be collected going toward the sun.
The typical radial position where these particles are turned to move again toward the sun is 5-10AU, depending on the energy. We think the key point that has been missed in the exospheric calculations is that the wrapped nature of the interplanetary field in the ecliptic introduces a longer arc length path to exit the heliospheric cavity than estimates based on the characteristic radial dimension of the cavity. This in turn implies that the Coulomb mean free path and the free path of any energy electron divided by the scale height along the magnetic field decreases with increasing distance; this in turn implies that it is inconsistent to neglect the backscatter of energetically unbound electron back into the heliospheric cavity. (Cf. Scudder and Olbert 1978b and Sittler et al. (1978) (this monograph) for further discussion on this point.)

To establish some contact with the parameter variation with the asymptotic solar wind speed which we noted in the introduction, we consider in Figure 6 a theoretical solution for an asymptotic solar wind speed of 800km/s. It can be shown in a rather general way that faster wind implies a higher electrostatic potential energy barrier for the coronal electrons to get to the 1AU observer. It is thus not surprising to see that the suprathermal populations are depleted relative to the thermal phase density-this was one of the strong anti-correlations which has been noted in the data.
If one compares this solution with that of Figure 4 we also see that the effective suprathermal

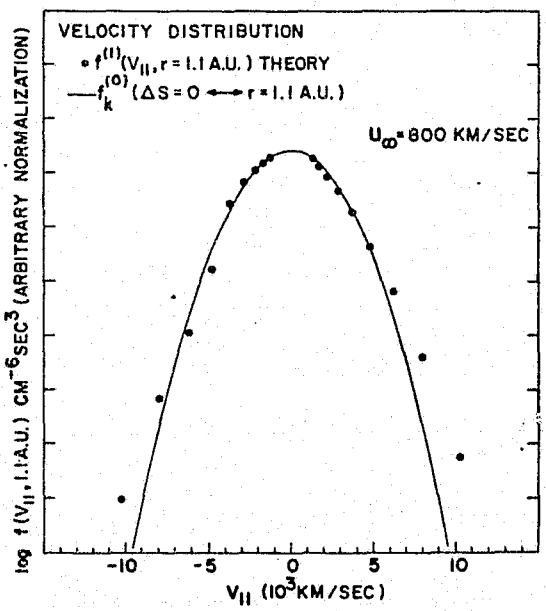


FIG. 6

"differential" temperature is lower in high speed wind than high. This is also a reported correlation in the solar wind electrons. The lower mean energy or differential "temperature" for the suprathermals in the high speed wind arises principally as a result of the dominant radial position of ballistic connection shifting into the upper corona (10-20R ) as a result of the enhanced barrier between the lower corona and the observer. Since the heat flux is an average over three properties of the distribution function: $Q = an_{skew}T_{skew}$ (skew), (where n is the number of particles carrying the heat, T is their effective mean energy, skew is the asymmetry of the heat carrying regime of $f(\underline{v})$, and a is a dimensionless constant of order 1), and all of these quantities are inversely correlated with the asymptotic bulk speed we immediately have that the local heat flux should be anti-correlated with the asymptotic bulk speed. This is a global relation and has none of the proximate character implied in the Fourier's heat law that is so commonly used. This latter anti-correlation has been reported at 1AU by Feldman et al. (1976) in another context and also reported by Rosenbauer et al. (1977) inside 1AU.

For lack of space in this monograph the details of the empirical corroborations of the expectations of this theory may be found in a forthcoming series of papers in the JGR: (Scudder and Olbert 1978a, 1978b).

CONCLUSIONS:

Fourier's law is certainly not a correct description for the transport of heat in an inhomogeneous plasma. The thermally driven stellar (solar) wind problem should be reposed. The principle impact will be for the acceleration region where perhaps inadequate estimates have been previously made for the rate at which internal energy can be supplied to the expanding flow. Coulomb collisions play an essential role in the transport physics of solar wind electrons.

The observation of a suprathermal population in an inhomogeneous plasma cannot be taken as a priori evidence of wave-particle interactions; by the nature of our construction we have excluded wave particle interactions, yet the combination of inhomogeneity and the Coulomb "window" above $E^*=7kT_c$ naturally gives rise to this leakage of non-local collisional populations in superposition with local

collisional populations. This is at odds with the Parker and Tidman (1958) suggestion that all suprathermal populations are generated as a result of Fermi or betatron action.

A theory necessary to show the global signatures in the in situ electron data is in its formative stages; these techniques have already suggested new ways to look at the data to extract information about the inaccessible regions of the solar wind expansion.

The theory that has been developed makes definite predictions, which have been corroborated. As an example the theory predicts (Scudder and Olbert, 1978b) the asymptotic radial variation for the electrons thermal temperature to be inverse 1/3 power as is supported by the Voyager 2 electron observations reported in this monograph by Sittler et al., (1978).

## ACKNOWLEDGMENTS

One of us (JS) would like to acknowledge discussions and/or manuscript comments by Drs. Acuna, Burlaga, Klimas, Ogilvie and Pizzo at NASA/GSFC and H. S. Bridge of MIT. (SO) has been supported in part by NASA Grant NGL-22-009-015.

## REFERENCES

Braginskii, S.I., "Transport Processes in a Plasma", Reviews of Plasma Physics, I, Consultants Bureau, New York, 1965.

Cohen, R. S., L. Spitzer, P. McR. Routly, "The Electrical Conductivity of an Ionized Gas," Phys. Rev., 80, 2, 230, 1950.

Feldman, W.C., J.R. Asbridge, S.J. Bame, M.D. Montgomery and S. P. Gary, "Solar Wind Electrons", J. Geophys. Res., 80, 31, 4181, 1975.

Feldman, W.C., J.R. Asbridge, S.J. Bame, and J.T. Gosling, "High Speed Solar Wind Parameters at 1 AU", J. Geophys. Res., 81, 28, 1976.

Gross, E. P. and M. Krook, "A Model for Collision Processes in Gases: Small Amplitude Oscillations of Charged Two-Component Systems", Phys. Rev., 102, 3, 1956.

Kopp, R. A. and F. Q. Orall, "Models of Coronal Holes above the Transition Region", in Coronal Holes and High Speed Wind Streams, J. B. Zirker, ed., Colorado Associated University Press, Boulder, CO, 1977.

Krall, N. A. and A. W. Trivelpiece, Principles of Plasma Physics, McGraw Hill Book Co., New York, 1973.

Lemaire, J. and M. Scherer, "Kinetic Models of the Solar and Polar Winds", Rev. Geophys. and Space Phys., 11, 2, 427, 1973.

Ogilvie, K.W. and J.D. Scudder, "The Radial Gradients and Collisional Properties of Solar Wind Electrons", J. Geophys. Res., 83, 3776, 1978.

Parker, E. N. and D. A. Tidman, "Suprathermal Particles," Phys. Rev 111, 5, 1206, 1958.

Rosenbauer, H. R., Schwenn, E. Marsch, B. Meyer, H. Miggenreider, M. D. Montgomery, K.H. Mühlhäuser, W. Pilipp, W. Voges, and S. M. Zink, "A Survey on Initial Results of the Helios Plasma Experiment", J. Geophys., 42, 561, 1977.

Scudder, J.D. and S. Olbert, "A Theory of Local and Global Processes Which Affect Solar Wind Electrons, I. The Origin of Typical 1 AU Velocity Distribution Functions--Steady State Theory", NASA TM 79621, August 1978, submitted JGR 1978a.

Scudder, J.D. and S. Olbert, "A Theory of Local and Global Processes Which Affect Solar Wind Electrons, II. Correlations of Thermal and Suprathermal Electrons with Local and Global Changes in the Interplanetary Medium", NASA TM 79628, August 1978, submitted JGR, 1978b.

Sittler, E.C., Jr., J.D. Scudder, J. Jessen , "Radial Variation of Solar Wind Thermal Electrons between 1.36 and 2.25 AU: Voyager 2", Proceedings Solar Wind 4; Burghausen, Springer Verlag, (this monograph), 1978.

# RADIAL VARIATION OF SOLAR WIND THERMAL ELECTRONS BETWEEN 1.36 AND 2.25 AU: VOYAGER 2

E. C. Sittler, Jr.*
J. D. Scudder
NASA/Goddard Space Flight Center
Laboratory for Extraterrestrial Physics
Greenbelt, MD 20771
and
J. Jessen
Center for Space Research
Massachusetts Institute of Technology
Cambridge, MA 02139

ABSTRACT Preliminary estimates of the electron core temperature as a function of radial distance from the sun between 1.36 and 2.25 AU are presented. The electron core temperature is found to gradually decrease with a power law index equal to $-0.34 \pm 0.16$.

## INSTRUMENT

The Voyager spacecraft plasma instruments measure solar wind electrons in addition to the ions as have been reported by Belcher et al. (1978) in this monograph. The electron sensor (see Figure 1 in Belcher et al., 1978) is a cylindrical, potential modulated Faraday cup, with aperture normal perpendicular to the radial and $23^{\circ}$ above the ecliptic plane. The field of view of the sensor is conical, with a half angle of $45^{\circ}$. The angle between the average Parker magnetic field direction and this normal is a decreasing function of the radial distance, with a maximum value of $45^{\circ}$ near earth and a minimum value of $23^{\circ}$ at 2.25 AU as the interplanetary magnetic field becomes increasingly transverse to the radial. The electron measurements are derived from fluxes which are locally directed away from the sun along magnetic tubes of force.

The electron sensors have two energy modes E1: 10 eV - 140 eV and E2: 140 eV - 5950 eV, each mode possessing 16 contiguously spaced energy channels with nearly equal widths of 320 km/s in speed. We will concentrate on the low energy regime in which the thermal component of the electrons are usually found. These are the first electron measurements which are differential, yet contiguous across the thermal plasma regime. This narrow spacing allows a determination of electron temperatures as low as $3 \times 10^{4}{}^{\circ}K$, where the electron thermal speed is 1000 km/sec.

Two samples of electron spectra from Voyager 2 data, acquired at 1.47 and 2.38 AU, respectively, are shown in Figure 1. These spectra were selected as they represent similar flow states of the solar wind at different radial distances. The actual macroscopic parameters are given beneath each figure. The ordinate of each spectrum is the reduced distribution function, $F_e(\underline{v} \cdot \hat{n})$, given by

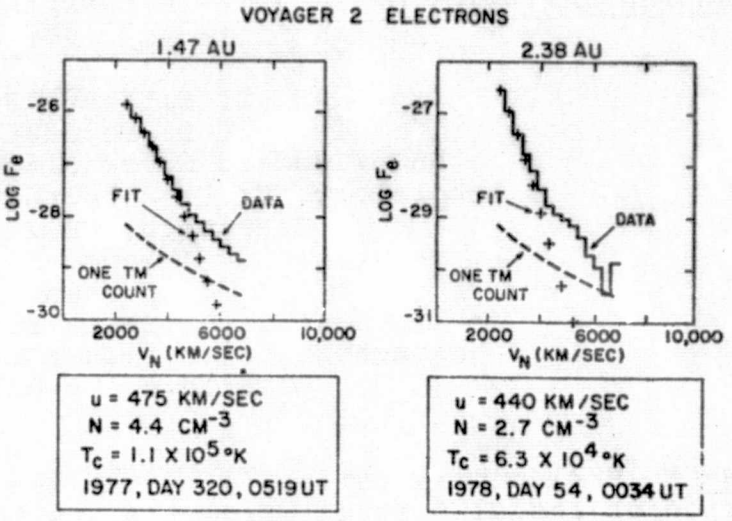


FIG. 1

$$F_e(v_n) = \frac{A\, I(v_n)}{v_n^3 \Delta v_n} \qquad v_n \equiv \langle \underline{v} \cdot \hat{n} \rangle \tag{1}$$

where $\hat{n}$ is the unit normal of the sensor, $v_n$ is the mean tuned speed, and A is a proportionality constant. The horizontal axis of each figure is the apparent speed of the detected electrons at the spacecraft. This speed is related to the ambient electron's speed $|v_d|$ before encountering the spacecraft sheath by the relation

$$|v_d| = \sqrt{v_n^2 - \frac{2e\Phi}{m_e}} \tag{2}$$

where $\Phi$ is the spacecraft's electrostatic potential with respect to the plasma. The solid line histogram form of the plotted data explicitly shows that the measured currents, $I(v_n)$ represent integrals over a speed range, $\Delta v_n$.

Since the current, I, collected by the detector represents a folding of instrument characteristics with the ambient properties, the reduced velocity distribution, $F_e(v_n)$ is not strictly proportional to the ambient phase density, $f_e(v_n)$. It can be shown that $F_e(v_n)$ is very similar to the actual velocity distribution. This is best illustrated by considering the crosses overlayed on this figure. The crosses represent the best fit convected Maxwellian, in the presence of a spacecraft potential, convolved with the instrument's response function for the thermal electrons (core). A Maxwellian in this format would

be a parabola. The convolution of the Maxwellian is almost indistinguishable from a parabola. We are thus justified in discussing the shape of $F_e(v_n)$ as being very nearly that of $f_e(v_n)$ so long as $f_e(\underline{v})$ does not have structures with half angles of less than $\sim 40^o$. In both spectra we see in $F_e(v_n)$ a characteristic low energy regime, where the convolved thermal Maxwellian (+'s) agree very well with the observations; these observations also show a non-Maxwellian suprathermal tail. For these two examples the departures from the thermal Maxwellian occurs at a speed for which the electrons have characteristic kinetic energies of $6 - 7kT_c$ where $T_c$ is the thermal temperature and k is Boltzmann's constant. The suprathermal electrons are almost always detectable above the one telemetry count threshold which itself generally represents an ambient signal larger than detector noise levels. In the more distant spectra the detector gain has been increased by a factor of 10, yielding a corresponding increase in sensitivity per telemetry count. These two representative examples clearly demonstrate the instruments capability to meaningfully measure and allow analysis of electrons many astronomical units from the sun; in this connection, as of this writing, Voyager 1 is acquiring electron data well above one telemetry count and instrument noise beyond 4 AU.

## ANALYSIS

We have determined ambient thermal electron parameters under the assumptions that: (1) the thermal electrons are well represented as an (isotropic) convected Maxwellian (2) and that the principal effect of the spacecraft potential on the sampled distribution function is that it is shifted in energy by the relation of equation (2) (cf., Sittler, 1978 for discussion of this point). The first assumption will be supported *a posteriori* by determining the local Coulomb mean free path over the scale height (Knudsen number) and showing that there are an increasingly adequate number of pitch angle scatterings to isotropize the thermal electrons. Because the core electrons dominate the electron density they cannot have a common bulk speed very different than that of the ions. This has been verified at 1 AU by Montgomery *et al.* (1968) and Feldman *et al.* (1975). The second assumption follows from an extension of Mott-Smith and Langmuir's (1927) results in the presence of highly subsonic flows (cf., Sittler, 1978). Since some attempts have been made to make the Voyager spacecrafts near iso-potentials to prevent arcing at Jupiter

encounters, we have an a posteriori check on the reasonable magnitude of the derived spacecraft potential. Once we have made these assumptions an analytical expression for $F_e(v_n, T_c, \Phi)$ can be written which is a non-linear functional of the core electron temperature, $T_c$, and the spacecraft potential, $\Phi$. The electron density is not a free parameter in our analysis, since we fixed the normalization of the Maxwellian by requiring it to equal the positive ionic charge density determined from the forward cluster ($n_e = n_p + 2\, n_\alpha$). We acquired a zeroth order estimate of $T_c^{(0)}$ as $(d\, \ell n\, F_e/dE)^{-1}/k$ where the logarithmic gradient is determined using the second and third speed channels. Note, the first energy channel has been temporarily omitted from our fits for now, since it has not yet been calibrated properly. We then use the first five measured channels (2-6) to determine, via gradient search, the optimal $T_c^{(n)}$ and $\Phi^{(n)}$. In general these five point fits were poor since the higher channels contained an admixture of suprathermal populations. We kept deleting the highest speed channel and redoing the fit until it was either $\chi^2$ acceptable or we were down to three points (one degree of freedom). In some instances when $T_c \lesssim 4 \times 10^4 {}^oK$, the three points fit were unacceptable and were omitted from subsequently averaged data. The reason for this difficulty which confined our analysis inside 2.25 AU is not due to the instrument's inability to resolve such a steep spectrum, but is due to the core electrons beginning to move inside the lowest energy channel as they cool. This effect is consistent with the scaling law for the breakpoint energy $E^* = 7kT_c$ proposed by Scudder and Olbert (1978). Because of this, one may have only one or two points characteristic of core electrons, while the remaining are characteristic of suprathermal electrons. This selection effect, which in our opinion does not seriously affect the current radial domain, would have caused our daily averages to be biased toward higher temperatures, especially at larger radial distances where the electrons are getting colder. When the first energy channel does become available our analysis will be carried out to larger radial distances.

An overview of the radial variation of thermal solar wind electron properties is presented in Figure 2. We have plotted daily averages of the Coulomb-Knudsen number ($\lambda_{mfp}/H$), the electron "core" temperature, $T_c$, the proton number density, $n_p$, and the solar wind (proton) speed. In support of our first assumption above we see that the Knudsen number is less than one for all stream conditions and in the radial interval has an average of 0.3. The scale height that has been used for the plotted Knudsen number is $H = (d\ \ell n\ n_e/dr)^{-1}$ is actually a lower bound, since the more appropriate scale height should be $H_{\|} = (d\ \ell n\ n_e/d\ \ell)^{-1}$ where the derivative is taken along the local magnetic field direction. These two facts imply that on average in this range the thermal electrons experience in excess of 4 collisions per scale length, $H_{\|}$, which is sufficient on theoretical grounds (Spitzer, 1953) to "Maxwellize" the core electrons. Although not shown for lack of space, the inferred, median spacecraft-plasma potential is 5.7 eV, consistent with theoretical estimates of this quantity for a conducting spacecraft surface in sunlight.

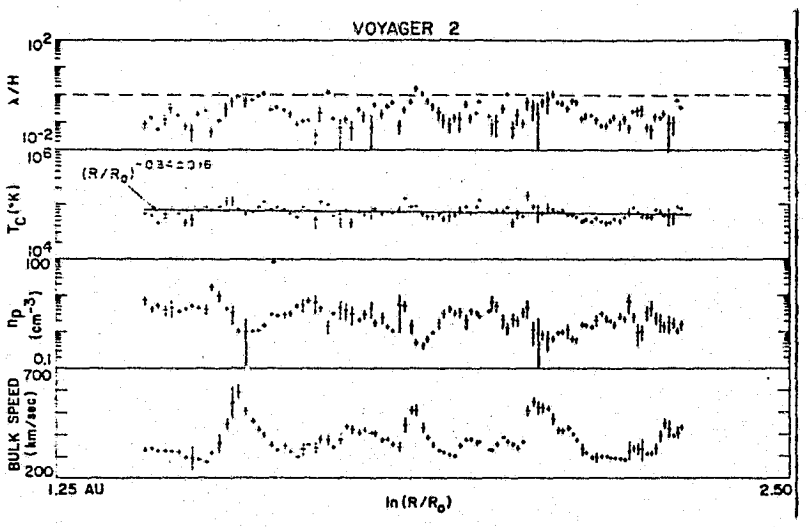


FIG. 2

The core temperature shows the usual compressive heating in stream interaction regions and the tendency to be locally cooler in high speed than low, that would be expected for its behavior like a classical gas (cf., Scudder and Olbert, 1978a,b). The electron core temperatures vary between $1.5 \times 10^{5o}$K and $4.5 \times 10^{4o}$K with an average value of $7.4 \times 10^{4o}$K, that is significantly lower than the mean value of $1.25 \pm 0.29 \times 10^{5o}$K reported by Feldman et al. (1975) based on 1 AU observations.

The daily average temperature data indicate as a whole a gradual decrease with radius, best fit (with formal errors) by an inverse power law with index $\alpha = 0.34 \pm 0.16$ and 1 AU intercept values of $T_c$ (1 AU) = $10^{4.94 \pm 0.05}$°K. In an effort to try to reduce stream interaction effects we also computed sliding linear least square fits to 3 data points which were spaced 26 days apart, none of which being within a leading edge of a stream. We thus obtained a distribution of slopes and intercepts giving a weighted mean inverse power law index of 0.47 and temperature at 1 AU equal to $9.8 \times 10^{4}$°K. These values happen to be in good agreement with our average fit to all the data. We also fit only the first two solar rotations of data to the power law relation to minimize the selection effect discussed previously. We obtained a power law index consistent with that reported for the entire three rotation fit.

A full analysis of this data set has not been completed. In order to present a timely preliminary survey for the Solar Wind 4 Conference all this data have been processed in the last two months. In time, a more thorough evaluation will be possible.

## DISCUSSION

The preliminary radial variation of the thermal electrons between 1.36 and 2.25 AU of $r^{-\alpha}$, $\alpha = 0.34 \pm 0.16$ is consistent with the recent determination of this quantity by Ogilvie and Scudder (1978) as determined from Mariner 10 data acquired between 0.4 and 0.85 AU, and as determined by Gringauz and Verigin (1975) between earth and orbit of Mars. This asymptotic variation in the core temperature is centered in the range (0.21 – 0.44) suggested by Scudder and Olbert (1978b) in order that the Coulomb collisional window at $E^* = 7kT_c$ be the local polarization potential energy to infinity. This radial variation appears to imply that the core is becoming more and more collisionless since the gas Knudsen number scales as

$$K_g = \frac{\lambda_{mfp}}{H} = \beta \frac{1}{r} \frac{T^2}{n} = \beta' \, r^{1-2\alpha}$$

for inverse square density variation and inverse power law index $\alpha$ for the temperature variation. If $\alpha < 0.5$ then $K_g$ grows with radius. The best fit $\alpha = 0.34$ seems to imply by this type of argument that the core will become less and less collisional with increasing radius. However, the magnetic Knudsen number for any latitude not over the solar spin axis goes as

$$K_M = \frac{\lambda_{mfp}}{H_{\|}} = \gamma r^{-2\alpha}$$

which decreases for any inverse temperature variation. We thus conclude that our data are consistent with an increasingly collisional character of the core electrons as r increases.

## ACKNOWLEDGMENTS

The authors acknowledge the contributions of H. S. Bridge, J. Belcher, S. Olbert, A. Lazarus, J. Sullivan, and G. Gordon of MIT in the design, fabrication, and analysis phases of the Voyager Plasma program, which have allowed us to determine our results. We also thank P. Harrison, D. Mead, L. Moriarity and F. Ottens of NASA/GSFC for ably assisting this data analysis effort in a timely fashion. (JJ) has been supported in part by JPL Contract 953-733.

## REFERENCES

Belcher, J. W., H. S. Bridge, A. J. Lazarus, and J. D. Sullivan, Preliminary results from the Voyager solar wind experiment, Proceedings Solar Wind 4 Conference, Burghausen, Federal Republic of Germany, Aug. 1978, Springer-Verlag, 1978, this monograph.

Feldman, W. C., J. R. Asbridge, S. J. Bame, M. D. Montgomery, and S. P. Gary, Solar wind electrons, J. Geophys. Res., 80, 4181, 1975.

Gringauz, K. J. and M. I. Verigin, Electron temperature radial distribution in solar wind and solar wind models, Space Research Institute, Academy of Sciences, USSR preprint, 1975.

Montgomery, M. D., S. J. Bame, and A. J. Hundhausen, Solar wind electrons: Vela 4 measurements, J. Geophys. Res., 73, 4999, 1968.

Mott-Smith, H. M. and I. Langmuir, The theory of collectors in gaseous discharges, Phys. Rev., 28, 727, 1927.

Ogilvie, K. W. and J. D. Scudder, The radial gradients and collisional properties of solar wind electrons, J. Geophys. Res., 83, 3776, 1978.

Scudder, J. D. and S. Olbert, A theory of local and global processes which affect solar wind electrons I. The origin of typical 1 AU velocity distribution functions - Steady state theory, NASA TM 79621, submitted to J. Geophys. Res., 1978a.

Scudder, J. D. and S. Olbert, II. Correlations of thermal and suprathermal electrons with local and global changes in the interplanetary medium, NASA TM 79628, submitted to J. Geophys. Res., 1978b.

Sittler, E. C., Jr., Ph. D. Dissertation, Massachusetts Institute of Technology, February 1978.

Spitzer, L., Jr. and R. Harm, Transport phenomena in a completely ionized gas, Phys. Rev., 89, 977, 1953.



*NAS/NRC Resident Research Associate

# OBSERVATIONS OF THE 'STRAHL' BY THE SOLAR WIND ELECTRON SPECTROMETER ON MARINER 10

K. W. Ogilvie
J. D. Scudder
NASA/Goddard Space Flight Center
Laboratory for Extraterrestrial Physics
Greenbelt, MD 20771

ABSTRACT A search of Mariner 10 electron data has been made for examples of unusual distribution functions, and three examples found which are identified with the "Strahl" previously described by Rosenbauer et al. (1976). The electron sprectrometer on Mariner 10 observed only electrons in motion towards the sun so the present results may be due to a "kinked" magnetic field geometry. The characteristic large increases in electron flux density at energies above about 50 eV appeared when the magnetic field direction was within the solid angle of the instrument and disappeared when this condition was no longer fulfilled. At other times and distances, the magnetic field direction was often within the solid angle of the instrument at times when no "Strahl" was observed. All three observations were made early in the encounter of the spacecraft with a high-speed stream, at heliocentric distances of between 0.65 and 0.45 AU. The angular response of the instrument is $\pm 3.5^{o}$ in the ecliptic plane and $\pm 13.5^{o}$ perpendicular to that plane, and contour plots indicate the "Strahl" to be a narrow feature with an energy dependent FWHM ranging between 13 degrees at 400 eV and $\sim 40^{o}$ at 50 eV, superimposed upon the normally quasi-isotropic halo part of the electron distribution function.

## INTRODUCTION

This paper will describe and interpret observations of a distortion of the interplanetary electron distribution function along the direction of the magnetic field. This distortion was first described by Rosenbauer et al. (1976), when discussing observations by the plasma instruments on the HELIOS spacecraft, and called by him the 'strahl'. The present observations were made by the plasma electron spectrometer on Mariner 10 (Ogilvie et al., 1977) at radial distances between 0.45 and 0.65 AU. This instrument scanned through an arc of $120^{o}$, from $\phi_{SE} = 140^{o}$ to $\phi_{SE} = 250^{o}$, Figure 1, about the anti-solar direction, and thus could only observe electrons in motion towards the sun. A search of the 90 days of data taken during the cruise from 1 AU to Mercury turned up at least three examples of the phenomenon. The relationship of this distortion to the magnetic field is illustrated by the fact that the strahl was only detected by Mariner 10 when the magnetic field vector passed within the sensitive cone of the instrument, bringing with it the axis of the strahl. The effect was not seen, however, every time the magnetic field direction was within

this cone. The examples of the strahl found in the Mariner 10 data supported the contention of Rosenbauer et al. (1976), that the strahl is usually found early in the observation of a high speed stream.

## OBSERVATIONS

The electron plasma instrument on Mariner 10 has been fully described by Ogilvie et al. (1977); the most important characteristics for the present purpose are the energy range (13.6 to 700 eV) and the angular resolution (+3.5 degrees in a plane perpendicular to the scan axis and +13.5 degrees in a plane containing the scan axis). The scanning motion was at a rate of one degree per second about an axis, Figure 1, perpendicular to the ecliptic plane. A 15 channel differential electron energy spectrum was taken once every six seconds. The Mariner 10 data was searched for spectra with abnormally high fluxes at high energies, and the events described here are part of the results of that search. Figure 2 shows the most extensive of the five observations, and the one from which the most information can be extracted. The top 5 panels are logarithmic plots of electron counting rates during a 3 1/2 hour period, measured when Mariner 10 was situated at a radial distance of 0.51 AU. At this time the

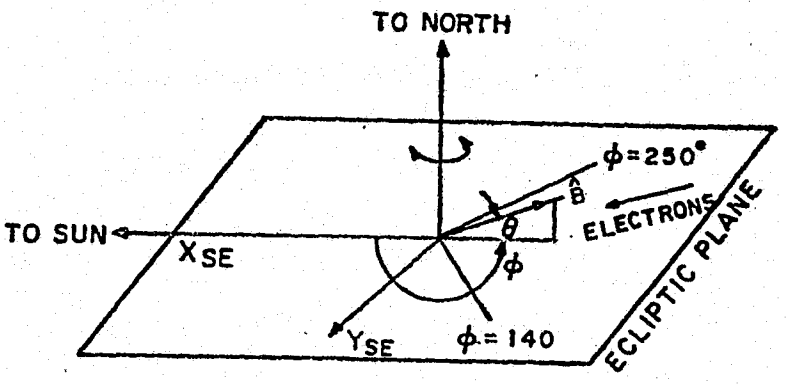


FIG. 1. The geometry of the detector scan. Electrons with velocity vectors falling inside the angular space $|\theta| < 13.5^{o}$, $\phi$ = 0 to 70 degrees and $\phi$ = 320 to zero degrees can enter the detector at some time during its angular scan. The scan axis points within a degree of North.

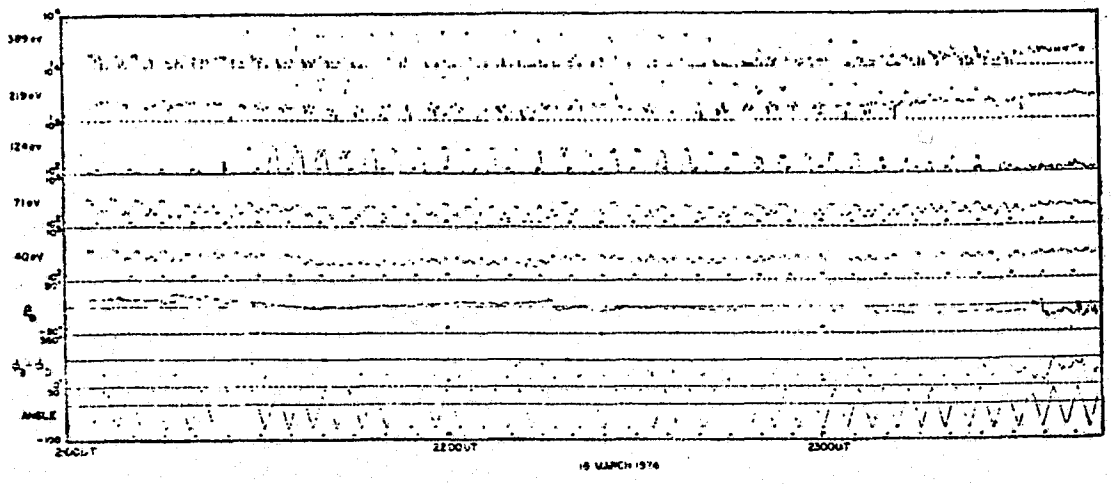

FIG. 2. Observation of strahl on March 16, 1975. The double peaks at the higher electron energies are caused by the scanning motion. The angle $\theta$ is the magnetic field latitude angle. The angle $\delta$ is the angle between the detector and the magnetic field $(\phi_B - \phi_D)$.

spacecraft had just encountered a compression region, and was situated in a positive magnetic sector. Until about 2130 UT the low energy channels (represented by the 40 eV and 71 eV channels in Figure 2) showed a small flux variation with scan angle but at higher energies (220 and 389 eV, for example) no such variation was present and the fluxes were low. Between 2115 and 2140 UT, the interplanetary magnetic field direction rotated slowly from a direction $\phi = 236^{\circ}$, $\theta = 30^{\circ}$, to a direction $\phi\ 335^{\circ}$, $\theta \simeq 0^{\circ}$. Electrons can enter the instrument at some time during its scan if their velocity vectors fall in the angular regions $\phi = 0$ to 70 degrees and $\phi = 320$ degrees to 0, $0 \leq \theta \leq$ 13.5 degrees, Figure 1, so that electrons aligned with the magnetic field could then be observed, and greatly increased highly anisotropic fluxes appeared in the higher energy channels; there was little change at lower energies. The characteristic double-peaked appearance at these energies is introduced by the motion of the detector, which traversed the velocity space structure twice in each angular scan. In response to a slow change in the magnetic field direction, to $\phi = 308^{\circ}$, $\theta = -26^{\circ}$, the flux of field aligned electrons again disappeared. We can see from Figure 1 that the angular width of the

strahl decreases as energy increases. Figure 3 shows a normalized logarithmic contour plot (of Log $[f/f_{15}]$) of the distribution function projected onto the ecliptic plane for a time period of three minutes at 2130 UT during this event. The quantity $f_{15}$ is the value of the distribution function derived from the lowest energy channel (13.6 eV). The vector labeled B represents the direction of the magnetic field, projected on the scan plane, and the shaded sector shows the angular width ($7^{o}$) of the instrument acceptance in this plane. One can see from Figure 3 that the apparent FWHM of the strahl, at an energy of 350 eV, is of order thirteen degrees, about twice the angular resolution of the instrument. Correcting for the non differential instrument response yields a value of $12.9^{o}$ for the FWHM. Thus the strahl appears as a distortion of the distribution function which can be measured at all energies but is most marked at several hundred electron volts, and therefore characteristic of the halo. It is very strongly correlated with the magnetic field direction. In Figure 4 we plot the distribution function along the axis of the feature and perpendicular to that

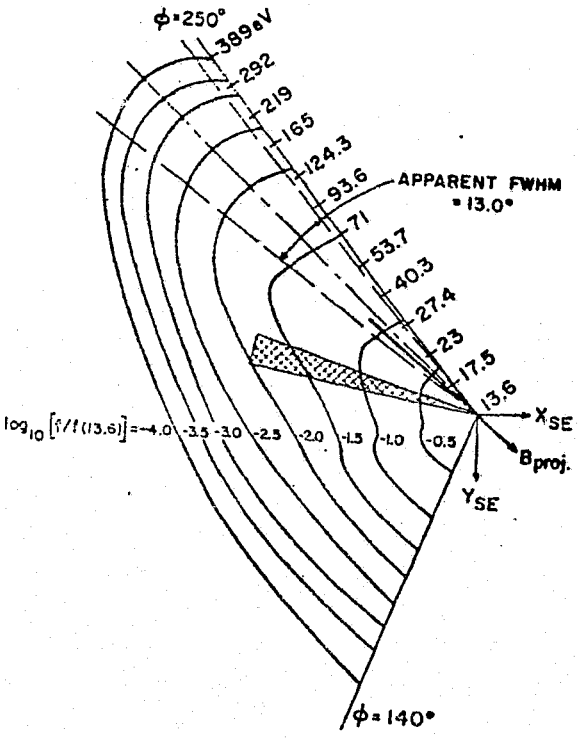


FIG. 3. Logarithmic contour plot of the electron distribution function for the event in Figure 2 at 2133 UT.

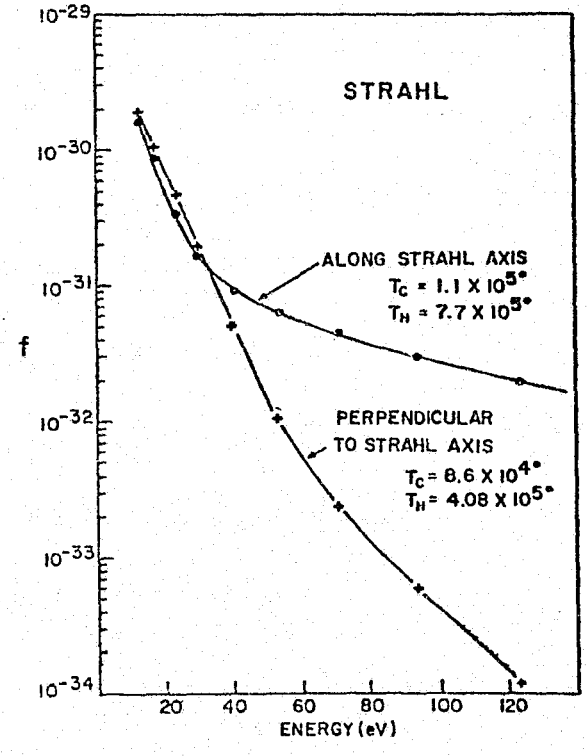


FIG. 4. The distribution function along the axis of the strahl and approximately perpendicular to it.

axis. We see that the differential temperature characterizing the core electrons up to 50 eV shows little change, while that of the higher energy electrons is almost twice as great along the axis as perpendicular to it. The distribution function also appears to be a better fit to a Maxwellian along the axis than perpendicular to it. In Figure 5 we see another example, an observation made on February 22, 1974, at a heliocentric distance of 0.635 AU in front of a high speed stream. There the magnetic field rotates from $\phi$ = 90 degrees, $\theta \simeq 0$ degrees to $\phi$ = 135 degrees $\theta$ = 0 degrees and back again. This is about five degrees less than required for the magnetic field direction to enter the instrument, but the anisotropic counting rate at high energies appears due to the finite velocity space width of the structure.

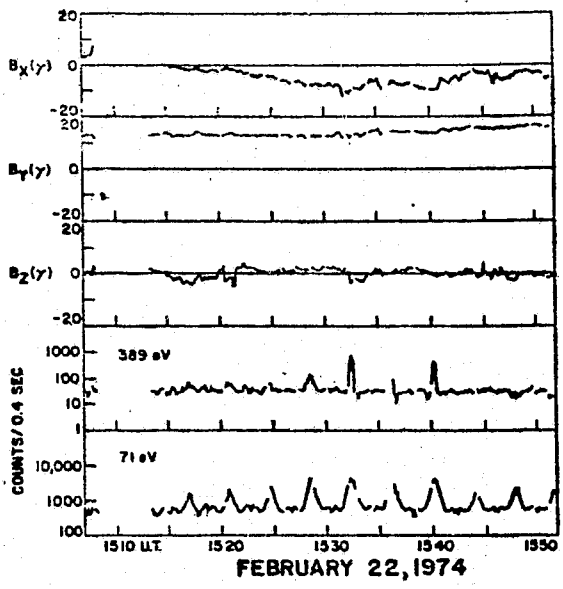


FIG. 5. An observation of a strahl on February 22, 1974.



Table I shows details of the five strahl detections; the search of the Mariner 10 observations during which these were found was conducted for unusually high counting rates at high energies. We cannot therefore state that no other strahl observations exist undetected in the data, but our purpose is not to survey general conditions of occurrence of the strahl, for which a sunward-facing instrument is obviously more suitable, but to use the angular resolution of the present instrument to study a few cases, primarily the March 16, 1974 observation shown in Figure 2.

TABLE I

| | Date | Radial Position | Relation to Stream | Remarks |
|---|---|---|---|---|
| 1. | Feb. 22, 1974 | 0.635 | Immediately before field maximum | Figure 5 |
| 2. | March 3-4, 1974 | 0.59 | Questionable | |
| 3. | March 16, 1977 | 0.51 | Immediately before field maximum | Figure 2 |
| 4. | March 22, 1974 | 0.45 | Immediately before field maximum | |
| 5. | March 24, 1977 | 0.48 | High bulk speed | |

## CONCLUSIONS

The observations show that electron distribution functions having distortions along the magnetic field direction can be observed by an anti-sunward facing detector. The angular half-width of the strahl decreases with increasing energy, with a FWHM value of 12.9 degrees at an energy of 350 eV, and the electrons measured along the magnetic field have a temperature of order $8 \times 10^5$°K. Such distribution functions are observed at positions close to the density increase at the leading edge of high-speed streams, in general agreement with Rosenbauer (1976). In Figure 6 we see two hypothetical geometrical arrangements leading to the observation of a strahl in the anti-solar direction. In each case the spacecraft is situated at the point X, just in front of the compression region of a high speed stream advancing towards the left. In the first case, a, the strahl is formed by electrons moving away from the sun in a kinked field configuration. The variation of the magnitude of the magnetic field along a field line passing through the point of observation is shown schematically in the B-L graph; the locally collisionless halo electron component forms the strahl in the region of decreasing magnetic field. In case b, there is no kinked field configuration, but electrons scattered back towards the sun at great distances are focussed into a strahl by moving from the higher magnetic field in the compression region into the region of lower magnetic field before it. This is again illustrated in the B-L graph inset into Figure 6b. A decision between these two possibilities must await the interpretation of more examples.

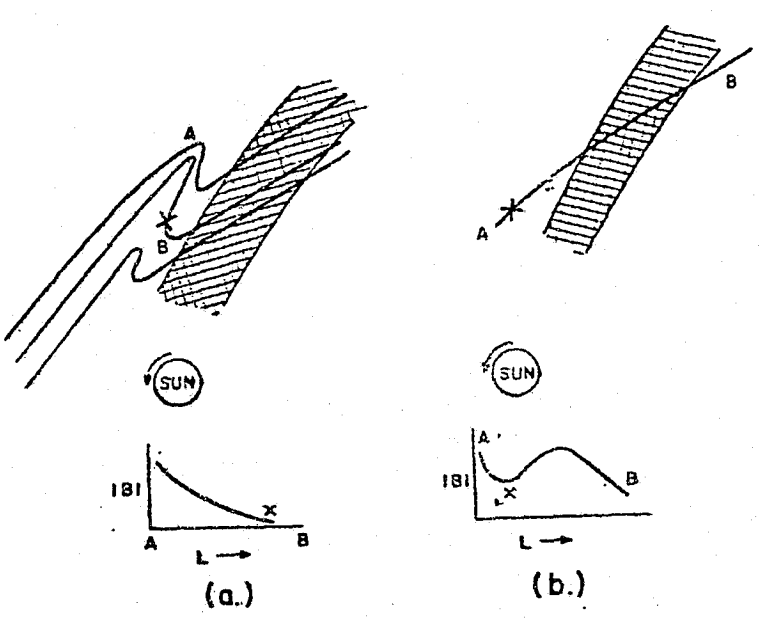


FIG. 6. Two possible magnetic field configurations which could be associated with the observation of a strahl in the cases described in this paper. The inset graphs indicate the variation of the magnetic field B along the arc-line L, going from A to B.

## REFERENCES

Ogilvie, K. W., J. D. Scudder, V. M. Vasyliunas, R. E. Hartle, and G. L. Siscoe, "Observations at the Planet Mercury by the Plasma Electron Experiment: Mariner 10", J. Geophys. Res., 82, 1807, 1977.

Rosenbauer, H., H. Miggenrieder, M. Montgomery, and R. Schwenn, "Preliminary Results of the Helios Plasma Measurements", Proceedings of International Symposium on Solar-terrestrial Physics, p. 319, D. J. Williams, ed., Am. Geophys. Union, 1976.

# An Evaluation of Corotating Solar Wind Stream Models

V. Pizzo
NAS/NRC Resident Research Associate
Laboratory for Extraterrestrial Physics
Goddard Space Flight Center
Greenbelt, Maryland 20771 USA

ABSTRACT

We compare the predictions of six nonlinear, single-fluid, corotating stream models ranging in sophistication from a one-dimensional hydrodynamic description (1-D HD) to the full three-dimensional magnetohydrodynamic (3-D MHD) formulation, for initial conditions at 0.3 AU intended to mimic the Helios close-pass data. It is shown that inclusion of both the multi-dimensional flow and the magnetic field are crucial to accurate description of the resulting stream evolution inside 1.0 AU. For most dynamical studies, the simpler 2-D MHD model will suffice. The full 3-D version is required only to investigate those properties strongly affected by the north-south flow.

Two main elements comprise any numerical simulation: first, the physical processes implicit in the equations used to describe the system; and second, the input conditions. Depending upon the input conditions, the relative importance of the physical mechanisms in the model can change dramatically. Therefore, before we can safely apply a model to the analysis of complex real data, it is necessary to engage in a systematic investigation into the properties of the model, using carefully chosen hypothetical examples that are both simple enough to facilitate analysis, yet realistic enough to touch upon the relevant physics of the system under study.

It is our purpose here to examine a family of basic single-fluid models of corotating structure in the solar wind--ranging in sophistication from a 1-D HD formulation to a 3-D MHD description--to see how the dimensionality of the formulation and the treatment of the magnetic field relate to the predictions forthcoming from these models.

Steady, corotating solar wind flow in the supersonic interplanetary regime may be approximately described by the MHD equations, presented here in vector form in the inertial frame:

$$-\Omega \frac{\partial \rho}{\partial \phi} + \nabla \cdot \rho \vec{u} = 0$$

$$-\Omega \frac{\partial \vec{u}}{\partial \phi} + (\vec{u}\cdot\nabla)\vec{u} = -\frac{1}{\rho}\nabla P + \frac{1}{4\pi\rho}(\nabla \times \vec{B})\times\vec{B} - \frac{G}{r^2}\hat{r}$$

$$\left(-\Omega\frac{\partial}{\partial \phi} + \vec{u}\cdot\nabla\right) P\rho^{-\gamma} = 0$$

$$\nabla \cdot \vec{B} = 0$$

$$-\Omega \frac{\partial \vec{B}}{\partial \phi} = \nabla \times (\vec{u} \times \vec{B})$$

The independent variables are the usual spherical coordinates ($r$, $\theta$, $\phi$), while the dependent variables are the velocity, $\vec{u}$, the density, $\rho$, the pressure, $P$, and the magnetic field, $\vec{B}$. The polytrope index, $\gamma$, is set at 5/3 in the examples presented here, $G$ is the solar gravitational constant, and $\Omega$ is the solar equatorial rotation rate. With the assumption of field-aligned flow in the rotating frame, the last (induction) equation may be eliminated entirely (except in the 1-D MHD formulation). Thus, in the full 3-D MHD case, we are faced with a coupled system of six hyperbolic, nonlinear, PDE's in three spacial variables. Details of the numerical techniques required to solve such systems may be found in Pizzo (1978a, b).

The essential physics embodied in these expressions is best viewed in the second (momentum) equation. The two terms on the left contain the basic kinematic steepening effect known as the stream interaction mechanism. (The $-\Omega\partial/\partial\phi$ term explicitly accounts for the exact relation between time and azimuth for corotating structure in the inertial frame.) The first two terms on the right describe the dynamical reaction of the plasma to these rotational-inertial forces. Thus, there exists a competition between the kinematic steepening mechanism on the one hand, and the dynamical broadening processes attributable to gas and magnetic pressure forces (and, to a lesser extent, magnetic tension) on the other.

Within the context of MHD models, the two main factors regulating the course of the dynamical evolution are the intensity of the field and the dimensionality of the formulation (the number of degrees of freedom allowed to the fluid motions). On this basis, we can establish a classification scheme encompassing six models, most of which, in some variation, have appeared before (1-D HD: Hundhausen, 1973; 1-D MHD: Steinolfson et al., 1975; 2-D HD: Goldstein, 1971; 2-D MHD: Nakagawa and Wellck, 1973, Goldstein and Jokipii, 1977, and Han, 1977; 3-D HD: Pizzo, 1978a; 3-D MHD: Riesebieter, 1977, and Pizzo, 1978b).

Our procedure will be to compare solutions obtained with each of the six models for identical input conditions, beginning at 0.3 AU and terminating at 1.0 AU. Thus the results of this paper apply only to stream dynamics inside earth orbit; a follow-on will deal with corotating structure in the distant solar wind, where the streams are highly evolved and shocks dominate the flow.

In Fig. 1, we show the input variations at 0.3 AU in radial velocity, $u_r$, number density, n, and temperature, T as a function of solar longitude. The nature of this hypothetical stream distribution--the narrow transition between the flow states and the marked intrinsic temperature-density-correlations--were chosen to mimic the Helios close-pass data (Rosenbauer et al., 1977). The other parameters, as appropriate in each model, were treated as follows: the gas pressure is held constant across the stream at the inner boundary, as is the field intensity ($|B| = 45\gamma$); the azimuthal velocity, $u_\phi$, is chosen such that the flow tubes in the rotating frame are all initially parallel; the meridional velocity, $u_\theta$, is set equal to zero; and the geometry of the 3-D distribution is a simple figure of revolution centered at the equator (i.e., circular contours on the source surface $r_o$ = 0.3 AU). For numerical convenience, we postulate periodic boundary conditions in the azimuthal direction. None of these latter parameter specifications seriously affect our results.

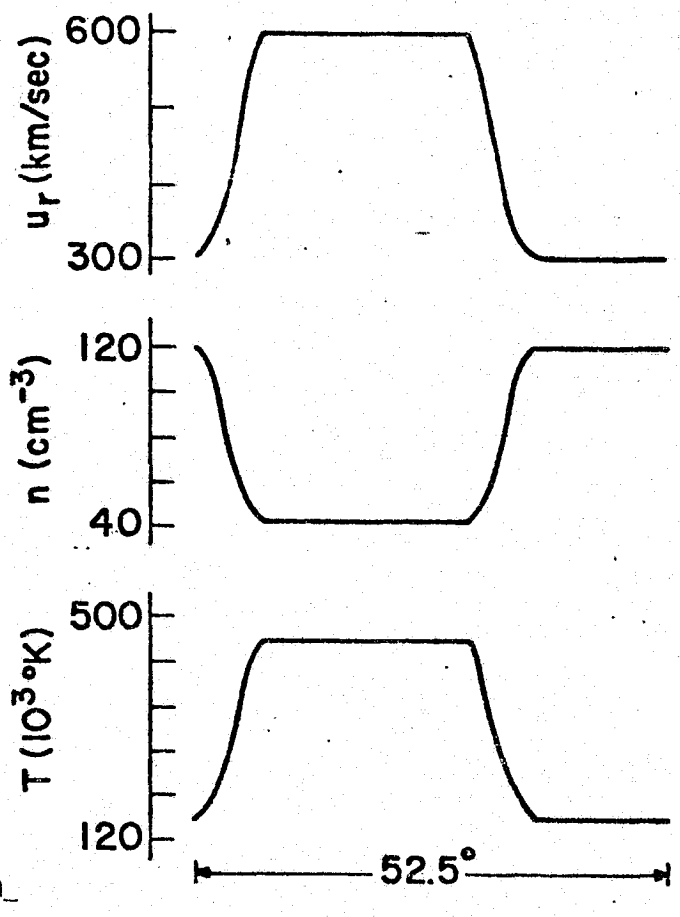


FIG. 1. SOURCE CONDITIONS AT 0.3 AU

Given these initial conditions at 0.3 AU, we use a finite-differencing form of the MHD equations to simulate the stream evolution to 1 AU. Figure 2 depicts solutions in the equatorial plane at 1 AU for the 1-D, 2-D, and 3-D MHD models. Just two parameters, the radial velocity and the number density, suffice to contrast the behavior of the models. We immediately see that the 3-D and 2-D solutions are quite similar, whereas the 1-D prediction is radically different. What has happened is that the nonradial flow in the multi-dimensional cases, though small ($u_\theta$, $u_\phi << u_r$), acts to smooth out the compression significantly. As the fluid is radially squeezed in the stream interaction, a vigorous shear flow develops at the interface between the fast and slow regimes, and the fluid slips laterally, thereby relieving the compressional stresses. This nonradial flow is not included in the 1-D description, and hence the evolutionary state of the stream is grossly overestimated. (In this case, the 1-D model predicts shock formation at about 0.4 AU, contrary to the observations, while the multi-D models shock near 1.2 AU.) Figure 2 also demonstrates that the burden of the nonradial flow effects are contained within the 2-D formulation; little is gained by expanding to 3-D. This behavior arises because the azimuthal flow is more directly driven by the rotational interaction than the meridional flow, which is of a decidedly subsidiary nature. The north-south transport of material spurred by the meridional motions has little effect upon the gross stream dynamics at any given latitude, except at the very fringes of the stream, where the amplitudes are low.

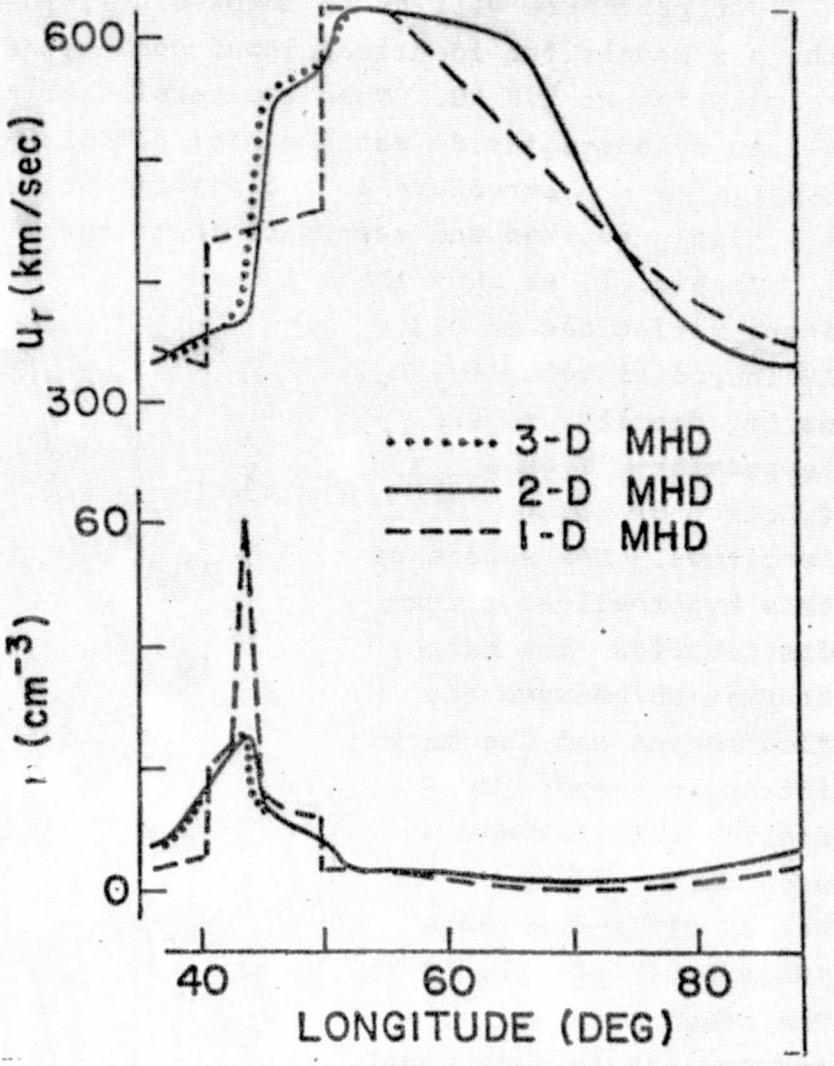


FIG. 2. DIMENSIONALITY EFFECTS (1 AU)

Fig. 2 is a direct measure of dimensionality effects in stream dynamics. However, an equally important question concerns the role of the smooth interplanetary magnetic field (IMF). Because the field is tied to the fluid motions and because the thermal and magnetic energy densities are comparable in the solar wind, we might expect magnetic effects to be significant in the interaction dynamics.

In Fig. 3, we isolate the magnetic influence by considering 2-D MHD (solid line, same as Fig. 2) and 2-D HD (dashed) solutions at 1 AU executed for the input conditions of Fig. 1. We see that, like the 1-D MHD model, the 2-D HD description overestimates the kinematic steepening, with a forward-reverse shock pair forming near 0.8 AU. (The compression region in the 2-D model is narrower than in the 1-D MHD at 1.0 AU since that of the latter shocked close to the sun and expanded thereafter.) The presence of the IMF approximately doubles the local characteristic speed at which disturbances propagate, thus spreading the stresses over a much larger area. Consequently, the magnetic field broadens the interaction structure not by a large increase in the nonradial flow velocities (which are nearly the same in the HD and MHD cases) but by distributing these deflections over a greater range.

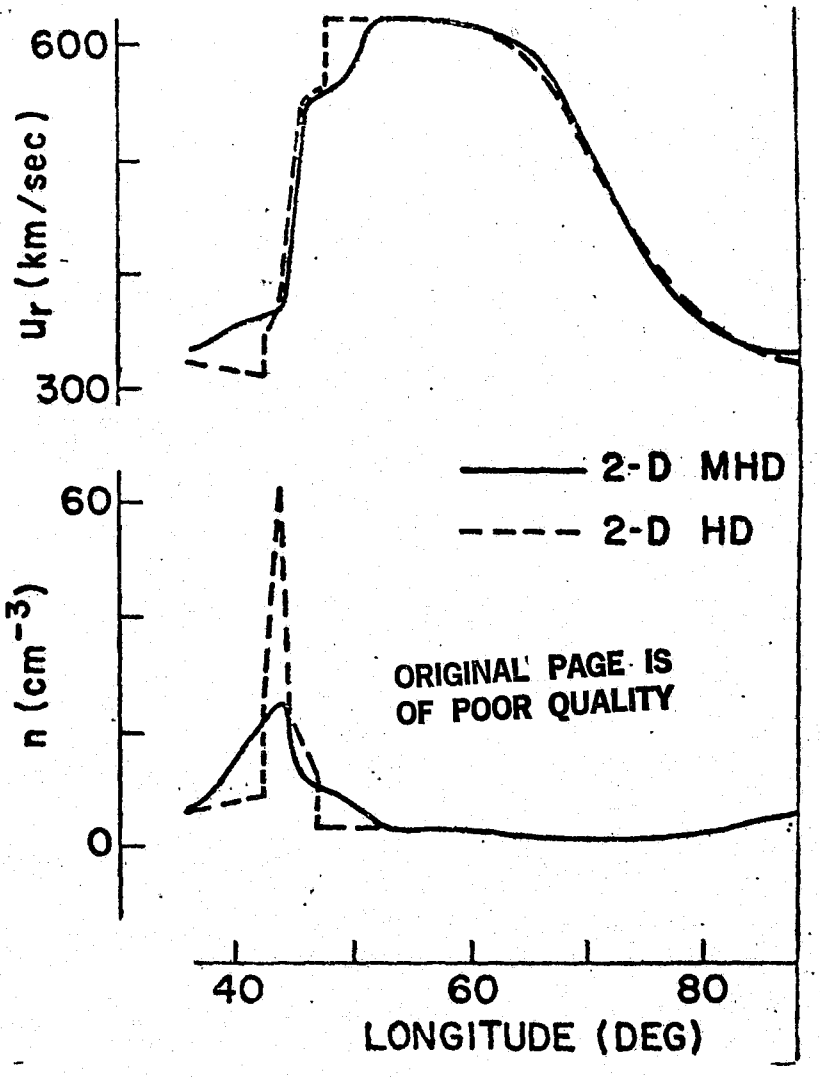


FIG. 3. MAGNETIC EFFECTS (1 AU)

For initially steep-sided streams, Figs. 2 and 3 demonstrate that dimensionality and magnetic effects act roughly on a par--neglect of either factor in a simplified model leads to gross misrepresentation of the evolutionary state of the stream near earth orbit. We do note, however, that inclusion of the IMF declines in importance (relative to the dimensionality) for streams having broader initial transitions between fast and slow flows (e.g., were the input variations more

nearly sinusoidal). In that case, the physical scale of the interaction region becomes so large that, even at the elevated magnetosonic speed, there is insufficient time for pressure signals to traverse the structure before it transits a substantial radial distance.

Thus the relatively economical 2-D MHD description emerges as the preferred vehicle for studying large-scale dynamics inside 1 AU and for experimenting with new physical processes (e.g., conduction, waves) in the structured solar wind. However, only the full 3-D formulation provides information on meridional flows, which are directly related to the unseen solar wind structure far from the ecliptic plane and which may have significant influence on the average angular momentum transport.

**ACKNOWLEDGMENTS:** The author wishes to thank L. Burlaga and J. Scudder for their helpful comments on this work.

## REFERENCES

Goldstein, B.E., Nonlinear corotating solar wind structure, CSR-P-71-63, Mass. Inst. of Tech., 1971.

Goldstein, B.E., and J.R. Jokipii, Effects of stream-associated fluctuations upon the radial variation of average solar wind parameters, JGR, 82, 1095, 1977.

Han, S.M., A numerical study of two dimensional time dependent magnetohydrodynamic flows, Ph.D. thesis, U. of Alabama in Huntsville, 1977.

Hundhausen, A.J., Nonlinear model of high-speed solar wind streams, JGR, 78, 1528, 1973.

Nakagawa, Y., and R.E. Wellck, Numerical studies of azimuthal modulations of the solar wind with magnetic fields, Solar Phys., 32, 257, 1973.

Pizzo, V., A three-dimensional model of corotating streams in the solar wind, I. Theoretical Foundations, JGR (in press), 1978a.

Pizzo, V., A three-dimensional model of corotating streams in the solar wind, III. Magnetohydrodynamic streams, JGR (in preparation), 1978b.

Riesebieter, W., Dreidimensionale modellrechnungen zum solaren wind, Ph.D. Thesis, TU Braunschweig, FRG, 1977.

Rosenbauer, H., R. Schwenn, E. Marsch, B. Meyer, H. Miggenrieder, M.D. Montgomery, K.H. Muhlhauser, W. Pilipp, W. Voges, and S.M. Zink, A survey of initial results of the Helios plasma experiment, J. Geophys., 42, 561, 1977.

Steinolfson, R.S., M. Dryer, Y. Nakagawa, Numerical MHD simulation of interplanetary shock pairs, JGR, 80, 1223, 1975.

# INVESTIGATION OF SECTOR BOUNDARY FINE STRUCTURE BETWEEN 0.3 AND 1 AU

K.W.Behannon and F.M.Neubauer
Inst. für Geophysik und Meteorologie der Techn. Univ.
3300 Braunschweig, F.R.G.

Abstract Sector boundary regions as seen in magnetic field data taken by Helios 1 between 0.3 and 1.0 AU during its primary mission were generally complex in structure, consisting of clusters of fine-scale directional transitions. The total field magnitude typically decreased in association with these directional discontinuities. The results of minimum variance analysis of 103 well-defined transitions show that the transition surface had a widely variable, at times perhaps oscillatory, local orientation. In 75% of the cases, the tilt of the surface relative to the ecliptic plane was found to be $> 45^{o}$. The transitions were generally most similar in magnetic characteristics to tangential discontinuities, although the results are not inconsistent with the observation of a small but nonzero normal component in at least half the cases studied.

## 1. INTRODUCTION

In spite of a great deal of work on the macroscopic aspects of magnetic sector structure over the past 14 years, very little has been done on the fine structure of the sector boundaries themselves. Studies to date (Smith, 1972; Bavassano et al., 1976) have presented results based on a relatively small number of boundary observations. A survey over a large number of observed boundary transitions shows that such transitions are usually more than just a single simple reversal of magnetic field polarity. They are often very complex in structure, consisting of a series of abrupt changes in field direction together with depressions in field magnitude. Thus, on the large scale, one is led to speak of "sector transition regions" in the observational data that consist of clusters of directional discontinuities and are also periods of relatively low and variable field strength.

This report presents some of the preliminary results from a comprehensive study of the sector transitions observed by the T.U. Braunschweig fluxgate magnetometer on Helios 1 (Musmann et al., 1975). Specifically, the data are from the primary mission period, December 1974 to April 1975, during which the spacecraft covered the heliocentric distance range $1.0 \leq r \leq 0.3$ A.U. The results to be described are from the minimum variance analysis of primarily 8 sec. average magnetic field vectors.

Before analysis results are presented, examples of data on several time scales, including the high resolution data (4 vectors/sec), will be

shown to illustrate both the large scale complexity and the fine-scale structure of sector transition regions. Quantitative results will then be described which address specifically

(1) fine-scale boundary orientation, and

(2) the type of discontinuity that best describes the fine-scale boundary.

There were two major magnetic sectors during the Helios 1 primary mission period, with at least two very narrow sector regions also visible (Neubauer, 1978). In the present study, eleven data intervals of from one to five days each have been analyzed. Within those intervals, a total of 103 fine-scale transitions were found which

(1) appeared to be sector boundary-associated by visual inspection of the data;

(2) had acceptably well-resolved variance ellipsoids (each case satisfied the criterion $\lambda_2/\lambda_3 \geq 2$, where $\lambda_2$ and $\lambda_3$ are the intermediate and minimum eigenvalues, respectively, determined in the minimum variance analysis); and

(3) had angles of rotation in the discontinuity plane $\omega \geq 120^{\circ}$ to differentiate them from ordinary directional discontinuities in the solar wind, since > 90% of such discontinuities are found to have $\omega < 120^{\circ}$ (Burlaga et al., 1977; Lepping and Behannon, 1977).

## 2. EXAMPLES OF TRANSITION REGION DATA

On the macroscale, the sector boundary which separated the two major magnetic sectors appeared to be a relatively simple-structured boundary. In fact, it was found on examination to have been complex in structure during the first and third times that it was observed and simple and sharply defined on the second and fourth recurrences. The complexity observed on passes one and three consisted not only of larger number of discontinuous rotations of the magnetic field, but also of periods of intermediate

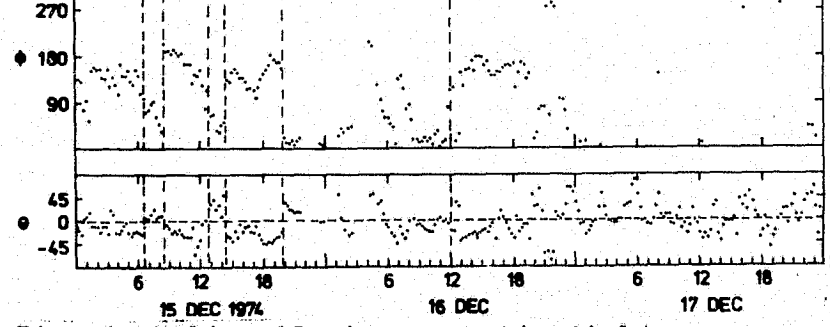


Fig. 1. Helios 15-min. magnetic field measurements of complex sector boundary near 1 AU. Data are field magnitude F, azimuth angle $\phi$ in ecliptic plane ($0^{\circ}$ toward sun), and elevation angle $\theta$ above and below ecliptic plane.

(non-spiral) field orientation.

Figure 1 shows 15-min. averages of field data taken during the first period at 0.98 AU. During the two days prior to the major change from "away" (-) to "toward" (+) orientation, the direction angles show that the field tended to alternate between the "away" spiral direction and a direction intermediate in azimuth between the "away" and "toward" directions. A tendency for alternation between positive and negative θ angles can also be seen. These data suggest that a series of possibly filamentary structures was observed in the sector transition region. A few large fluctuations in direction were also observed to occur after the main, macroscale polarity reversal. In all, 13 individual transitions that satisfied the above-listed selection criteria were found during the period shown, some of them corresponding to the "filament" boundaries seen in the 15-min. averages.

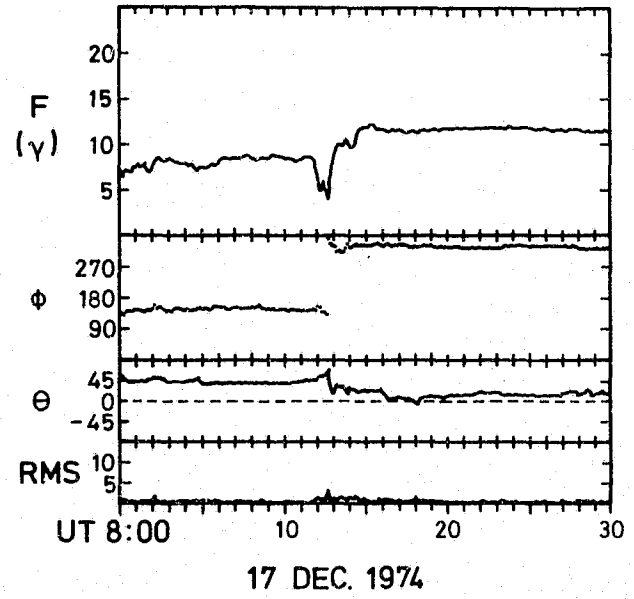


Fig. 2. Helios 8-sec. averaged data showing fine-scale sector transition. In addition to field magnitude and direction, RMS deviation of magnitude F is also given.

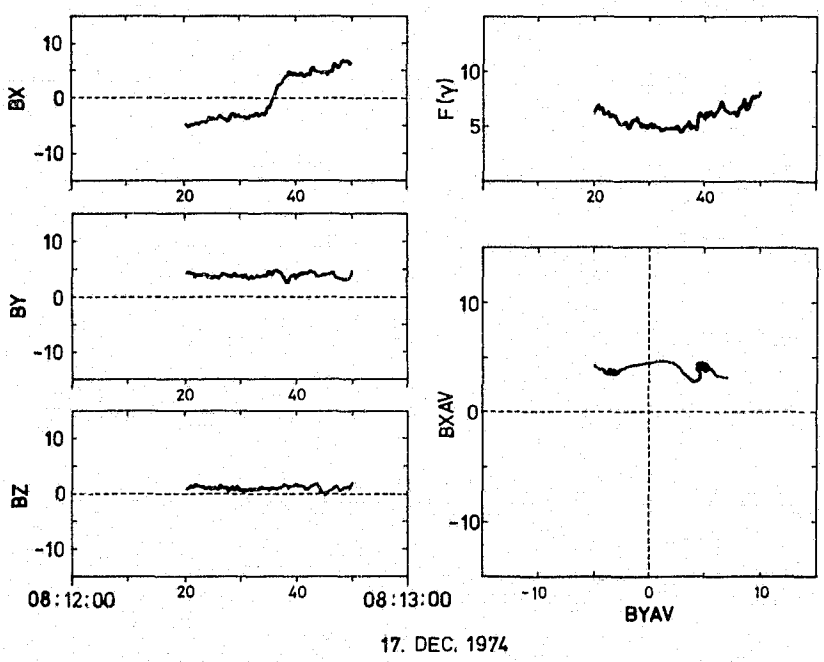


Fig. 3. Detailed (250 msec) measurements of transition shown in Figure 2. BZ is field component in minimum variance direction; BX and BY are in maximum and intermediate variance directions. Hodograph shows smoothed XY-plane variation of field (1-sec. averages).

Figure 2 shows one-half hour of 8-sec. average data that include a typical fine-scale transition, in this case from positive to negative sector polarity. The field magnitude is seen to be reduced significantly

during the relatively sharp direction change.

Figure 3 shows the most detailed data for this transition. One sees in this case a small but persistent normal component, $B_Z$ ($\langle B_Z \rangle = 1{\cdot}4\gamma$). The continuous change in magnitude during the transition results in the roughly linear rather than circular appearance of the hodograph.

## 3. ANALYSIS RESULTS

1. A major subject of interest in this investigation concerned the orientations of the fine-scale transition boundaries studied. Minimum variance analysis yielded an estimate of the normal vector orientation in each case. Figures 4a and b show examples of these results for two different boundary transitions in terms of the $\theta,\phi$ coordinates of the tip of the unit normal vector. For each example, arrows mark the azimuthal angle values of the directions perpendicular to the average observed field azimuth angle, $\phi_B$, and to the spiral direction, $\alpha_p$, calculated from the mean solar wind speed. The points plotted have been coded according to the value of the eigenvalue ratio, $\lambda_2/\lambda_3$, previously defined.

In Figure 4a the results for the transitions comprising the boundary region shown in Figure 1 are given. Although the set of normal directions in this case are spread over ranges of $110^0$ in $\theta$ and $99^0$ in $\phi$, a tendency is seen in the majority of cases for recurrence of an azimuthal orientation centered roughly half way (within $\pm$ $20^0$) between the radial direction and the direction perpendicular to the spiral field direction. Some oscillation of the $\theta$ angle is also seen, although in only three cases were negative values obtained.

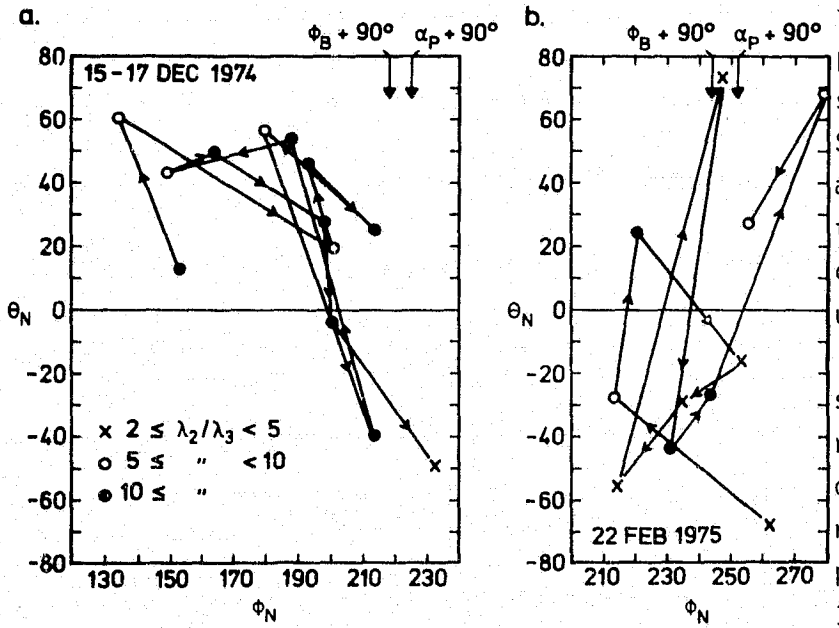


Fig. 4. Orientations in elevation and azimuth of collective transition surface normal vectors for sector transition periods (a) near 1 AU and (b) at 0.52 AU. For symbol definition see text.

Figure 4b shows results from a transition region which consisted on the macroscale of a negative-to-positive polarity change, with 11 fine-scale transitions satisfying the selection criteria. Here the normal orientations

were scattered about an azimuthal direction roughly perpendicular to the average spiral direction. There was also an oscillatory deflection of the normals often to large elevation angles, both positive and negative. Such data are consistent with a model of the boundary in which the surface is rippled or corrugated.

A statistical study over all 103 fine-scale transitions being considered in this investigation shows that $\langle\theta_n\rangle \simeq 0^o$, with $|\theta_n| < 45^o$ in 75% of the cases and $\langle|\theta_n|\rangle = 32^o \pm 21^o$, which means that the fine scale boundary surface was predominately oriented at an angle $> 45^o$ to the ecliptic plane. The wide variability seen in fine-scale boundary orientation makes it difficult, if not impossible, to infer an average orientation or "tilt" for the macroscale current sheet from such observations.

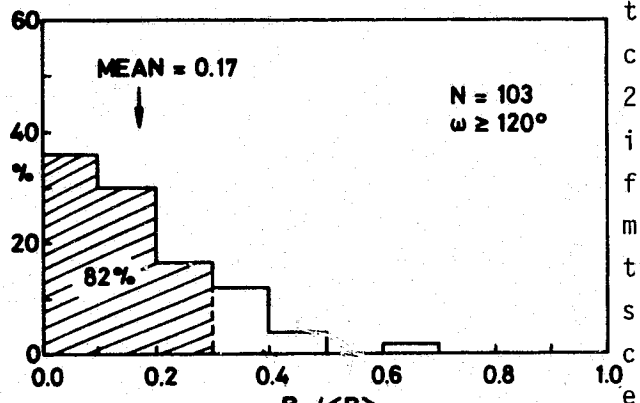


Fig. 5. Percent distribution of magnitudes of sector transition surface normal vectors relative to average total field in each case.

2. The second major point of interest in the investigation was the identification of the type of discontinuity most consistent with the fine-scale transition observations. Figure 5 shows the distribution of normal component magnitudes, normalized in each case by the average total field magnitude, i.e., $|B_n|/B_o$. As can be seen, 82% of the cases had $|B_n|/B_o \leq 0.3$, a significantly larger fraction than is found in general for ordinary directional discontinuities in the solar wind (see review by Neubauer and Barnstorf, 1978). In particular, few cases were found which were consistent with "large-$|B_n|/B_o$" rotational discontinuities. On the other hand, by conservative estimate approximately half the cases yielded normal component magnitudes which were larger than one would expect for a truly zero normal, when possible measurement and computational errors are considered.

## 4. SUMMARY

A study of the sector transitions observed during the primary mission of Helios 1 shows that such transitions were generally "complex" rather than "simple" in structure on the fine-scale. Results suggest that the boundary surface may at times have had a locally irregular or "corrugated" structure, since

a. the transition regions were observed to be composed primarily of clu-

sters of discontinuities;

b. the tilt of the discontinuity surfaces was found to be > $45^{o}$ on average; and

c. coherent patterns of oscillation of the transition surface normal direction were sometimes seen.

It is concluded that the fine-scale boundary is more nearly "TD-like" "RD-like" on average on the basis of

a. the generally small magnitude found for the component normal to the boundary surfaces, and

b. the observation usually of "dips" in total field magnitude in association with the directional discontinuities.

For at least half the cases studied the results were not inconsistent with the existence of a small, nonzero normal component as required, for example, for reconnection.

## 5. REFERENCES


Bavassano, B., M. Dobrowolny, and F. Mariani, Evidence of magnetic field line merging in the solar wind, J. Geophys. Res., 81, 1, 1978.

Burlaga, L.F., Microscale structure in the interplanetary medium, Solar Phys., 4, 67, 1968.

Burlaga, L.F., J.F. Lemaire, and J.M. Turner, Interplanetary current sheets at 1 A.U., J. Geophys. Res., 82, 3191, 1977.

Lepping, R.P. and K.W. Behannon, Characteristics of directional discontinuities between 0.46 and 1.0 A.U. (Abstract), EOS Trans. AGU, 58, 486, 1977.

Musmann, G., F.M. Neubauer, A. Maier, and E. Lammers, Das Förstersonden-Magnetfeldexperiment (E2), Raumfahrtforschung, 19, 232, 1975.

Neubauer, F.M., Recent results on the sector structure of the interplanetary magnetic field, in Proceedings of the Second European Solar Meeting "Highlights of Solar Physics", Toulouse, France, 8-10 March, 1978, in press.

Neubauer, F.M., and H. Barnstorf, Recent observations and theoretical results on tangential discontinuities in the solar wind, Solar Wind 4 Conference, Burghausen, FRG, 1978.

Smith, E.J., Comments on sector boundaries, Solar Wind, NASA SP-308, 469, 1972.

# BIBLIOGRAPHIC DATA SHEET

| 1. Report No. TM 79711 | 2. Government Accession No. | 3. Recipient's Catalog No. |
|---|---|---|
| 4. Title and Subtitle Contributions to the Fourth Solar Wind Conference | | 5. Report Date |
| | | 6. Performing Organization Code |
| 7. Author(s) M. Acuna, K. Behannon, L. Burlaga, R. Lepping, N. Ness, K. Ogilvie, V. Pizzo, J. Scudder, E. Sittler | | 8. Performing Organization Report No. |
| 9. Performing Organization Name and Address NASA/GSFC Laboratory for Extraterrestrial Physics Interplanetary Physics Branch, Code 692 Greenbelt, MD 20771 | | 10. Work Unit No. |
| | | 11. Contract or Grant No. |
| | | 13. Type of Report and Period Covered Technical Memorandum |
| 12. Sponsoring Agency Name and Address | | 14. Sponsoring Agency Code |
| 15. Supplementary Notes | | |

16. Abstract. This report contains a collection of papers discussing some of the most recent results in interplanetary physics. These include observations of shock waves and post-shock magnetic fields made by Voyager 1, 2; observations of the electron temperature as a function of distance between 1.36 AU and 2.25 AU; and observations of the structure of sector boundaries observed by Helios 1. A theory of electron energy transport in the collisionless solar wind is presented, and it is compared with observations. The report also contains a review of the theory and observations of Alfven waves and Alfvenic fluctuations in the solar wind.

| 17. Key Words (Selected by Author(s)) | 18. Distribution Statement |
|---|---|
| Interplanetary magnetic fields, interplanetary plasma, solar wind | |

| 19. Security Classif. (of this report) | 20. Security Classif. (of this page) | 21. No. of Pages | 22. Price* |
|---|---|---|---|
| U | U | 69 | |

*For sale by the National Technical Information Service, Springfield, Virginia 22151.